

**AVHRR PIXEL LEVEL CLEAR-SKY CLASSIFICATION USING
DYNAMIC THRESHOLDS (CLAVR-3)**

S.Vemury¹, L. Stowe² and V.Anne¹

To be submitted to

Journal of Atmospheric and Oceanic Technology

Final version 9 (draft 7)

December 1998

1. Scientific Management & Applied
Research Technologies, Inc.
8401 Corporate Drive, #430
Landover, MD 20785
2. NOAA/NESDIS
NOAA Science Center
5200 Auth Road
Camp Springs, MD, 20233

ABSTRACT

Clear-sky classifications from the Clouds from AVHRR-Phase 1 (CLAVR-1) program are used to create an 8-day rotating Clear-sky Radiation Data Set (CRDS8). This data set is used to create satellite zenith angle dependent, dynamic albedo and temperature prediction models for ocean and six different vegetation index groups in 10° latitude intervals over the globe. Individual pixels from ambiguously classified 2x2 pixel arrays from CLAVR-1 (MIXED and RESTORED-CLEAR) are re-examined at the individual pixel level, using these dynamic clear-sky thresholds from the prediction models, and are reclassified as CLEAR, MIXED or CLOUDY. This methodology is referred to as the CLAVR-3 algorithm. Many of the MIXED (partially cloudy or mixed overcast) pixels from CLAVR-1 are found to be cloud-free after using the dynamic thresholds. Similarly, a number of RESTORED-CLEAR pixels actually belong to the mixed category, while some are truly CLEAR.

Many of the clear/cloud classifications from CLAVR-1 2x2 pixel array method are uncertain due to the use of spatial uniformity tests and universal (constant) thresholds in its multi-spectral sequence of tests. Results from the CLAVR-3 pixel level dynamic threshold method demonstrate that many of these uncertain classifications are likely to be CLEAR. CLAVR-1 problems that could be resolved with the current clear sky statistics as well as those that can be corrected with further improvements in the method, have been identified.

The CLAVR-3 reclassification using zonal, surface type and angle dependent dynamic thresholds described here leads to a 75% increase in clear pixel populations globally during the ascending part (mostly daytime portion) of orbits and a 94.9% increase during the descending part (mostly nighttime). When mapped into equal area grid cells, many more grid cells were found to contain clear radiance statistics, increasing the CLEAR grid cell populations by 19.3% globally, and by 12.5% and 23.8% over land and ocean, respectively, for ascending data. The percentage of grid cells that have CLEAR data during ascending segment, increased from 54.5% in CLAVR-1 to 65% in CLAVR-3. Maps of differences in equivalent-isotropic albedo and brightness temperature for grid cells containing clear pixels before and after application of CLAVR-3 are used, as well as histogram analyses, to demonstrate the quality of clear pixels derived from the CLAVR-3 algorithm. These analyses show that the quality of CLEAR pixels is maintained under CLAVR-3. The CLEAR sample from CLAVR-1 represents a subset of the total sample of PURE CLEAR. The addition of new CLEAR pixels over oceans from CLAVR-3 tends to enhance the CLEAR albedos and diminish the CLEAR brightness temperatures slightly. The possibility that this enhancement is a result of slight cloud contamination will be the subject of future investigations. Based on the results presented, we conclude that the CLAVR-3 algorithm concept, after some additional adjustments and validation, can be used to enhance the spatial coverage of remotely sensed operational land, ocean and atmospheric parameters that depend on clear-sky radiance observations from AVHRR.

1.0 INTRODUCTION

Cloud detection, specification and screening using satellite measurements are potentially valuable for providing observations useful for studies of climate and weather forecasting. Clouds from AVHRR (CLAVR) is a NOAA/NESDIS four phase program with the objective to develop a unified technique for cloud screening and for cloud detection using all five channels of the Advanced Very High Resolution Radiometer (AVHRR) on the NOAA polar orbiting satellites. Three of four phases of the CLAVR program have been developed. The objective of Phase 3 of CLAVR is to improve the quantity of clear-sky observations from Phase 1 of CLAVR, while maintaining the quality of those classifications. The phase 1 CLAVR (CLAVR-1) algorithm is described in Stowe et al. (Stowe, et al., 1991; 1999). Some additional analyses of resulting estimates of cloud cover from CLAVR-1 have been described by Hou et al., (1993), Stowe et al. (1995), and by Luo, et al, (1999). Some unique clear-sky pixel classification methods have also been developed for the Phase-2 CLAVR algorithm, and will be the subject of a subsequent publication, Davis, et al., 1999. The fourth phase deals with derivation of cloud optical and physical properties from cloud layer radiances emerging from CLAVR-2, and is still under development.

A 2x2 pixel array classification scheme for AVHRR global area coverage (GAC) data was used in CLAVR-1, with the objective of separating clear pixel arrays from partially and fully cloudy ones using a reliable multi-spectral classification scheme. The classifications are based on a fairly conservative sequence of threshold tests applied to spectral equivalent-isotropic albedo and brightness temperature values, their spectral differences, and their spatial uniformity (Stowe, et al., 1999). Pixel arrays that could not

be unambiguously classified were put either into a MIXED (partially cloudy or mixed overcast) or RESTORED-CLEAR category.

A variety of techniques exist in the published literature for screening clouds. The purpose of screening techniques is to identify the presence of cloud in the pixel field of view, and to eliminate the pixel from further consideration. These methods are used to derive surface (land or ocean) characteristics. Such techniques are very useful in specifying land cover types, particularly vegetation (DeFries, Hansen and Townshend, 1995), and for the determination of sea surface temperatures (SSTs; McMillin and Crosby, 1984; McClain et al., 1985; Antoine et al. 1992). For land applications, clear sky data from CLAVR-1 method were evaluated by Gutman and Ignatov (1996) who clearly demonstrated the importance and usefulness of CLAVR-1 clear-sky flags in improving the quality of clear sky data sets over land.

Screening algorithms use bi-spectral (visible and infrared), and visible or IR alone threshold techniques and have been discussed extensively in the literature. Both albedo and temperature are generally viewing angle and illumination angle dependent. Illumination geometry varies greatly as you move over different latitude bands. The effect of this solar zenith angle variation and the resulting variations in thresholds for albedo and temperature have been investigated by Hutchison et al. (1995). They have not, however, considered the effect of satellite zenith angle, which generally varies between -60° to $+60^\circ$ over the repeat cycle of the polar orbiting satellites. Wu et al. (1995) developed bi-directional reflectance distribution functions (BRDFs) using high resolution local area coverage (LAC) pixels at 1 km resolution. For specific locations over the continental U.S. and Canada, they studied the variation of BRDFs with land

type, as given by the Normalized Difference Vegetation Index (NDVI), and solar zenith angle. BRDF models for global applications were previously developed by Taylor and Stowe (1984) and Suttles et al., (1988). But those models were generated from broadband relatively large field of view (near 100 km.) sensors used for measuring Earth's radiation budget. The models thus are not directly applicable to the narrow band scanners on AVHRR. Stowe et al. (1993) developed such models from AVHRR spectral channel measurements that depend on satellite zenith angle at the grid cell level and reported on their applications over the globe. Further improvement in global classification of CLEAR beyond CLAVR-1 is only possible if the GAC pixels can be classified individually and also if fixed thresholds are replaced by variable cloud/no-cloud thresholds which depend on time, latitude, viewing and illumination geometry, and meteorological factors. The purpose of this work is to incorporate these two improvements - pixel level classification and use of dynamic thresholds, into CLAVR. Development of such clear-sky radiation thresholds involves construction of clear sky albedo and temperature fields, which provide regional, dynamic prediction models (Stowe et al., 1993). The models then yield estimates of predicted clear-sky albedo and temperature which can be used as dynamic thresholds. These are used to improve the quantity while maintaining the quality of clear-sky pixel classifications.

NOAA polar orbiting satellites have a repeat cycle which varies between 6 and 10 days, depending on the orbit and the lifetime of the satellite. A region viewed on day 1 at a particular satellite zenith angle (SZA) returns to the same angle after 8 days in the case of a 8-day repeat cycle. During the 8 days, the region would be viewed by the radiometer from different SZAs, until it comes back on the 9th day to be 'in phase' with

the 1st day (Gutman, 1989). This permits the inclusion of effects of SZA variation into the dynamical models.

In brief, the methodology developed here is as follows. From 2x2 pixel array CLEAR classifications of CLAVR-1, a daily Clear-sky Radiation Data Set (CRDS) containing clear-sky radiation statistics, is created. Such clear sky radiation data statistics from 8 successive days (called CRDS8) from a satellite with an 8-day repeat cycle provide variation of means and standard deviations of albedo and temperature for each region containing clear samples. Since these regions are viewed at different angles during the 8 successive days, the CRDS8 provides angle dependent means and standard deviations for all regions with clear sky conditions.

Such bidirectional reflectance and emission functions developed from CRDS8, were presented by Stowe et al., 1993, Vemury et al. 1997 for the current application. These bidirectional functions provide desired dynamic and angle dependent thresholds. These thresholds are then used in CLAVR-3 to reassess the prior classification of "uncertain" pixels from CLAVR-1.

Section 2 defines the nature and describes the magnitude of "uncertain" pixels under the 2x2 pixel array classification scheme used in CLAVR-1. Details on the construction of the CRDS8 data sets and methods to build regional angular dependence models (ADMs) for albedo and temperature from CRDS8 are presented in section 3. Section 4 describes the dynamic prediction models developed from the regional models and focuses on the algorithm used to reclassify "uncertain" pixels from CLAVR-1. The improvements obtained using the present reclassification methodology

are presented in Section 5. A brief description of future enhancements that can be implemented in the classification methodology under CLAVR-3 is included in Section 6 together with conclusions.

A complete month of AVHRR data for September 1989 from the NOAA/11 satellite have been classified by CLAVR-1 for testing of the CLAVR-3 methodology. One day (Sept. 9, 1989 (89252)) from the daily data sets derived using the present pixel level and dynamic threshold scheme (CLAVR-3) applied to the last 22 days of the month, has been used in the analyses presented here.

2. CLAVR-1 CLASSIFICATION AND IMPLICATIONS FOR CLAVR-3

Two categories of pixels from CLAVR-1 contribute to the uncertainty in classification, both of which are addressed in this paper. They are: i) the uncertain pixels in the MIXED category which have resulted from two factors described below; and ii) pixels in the RESTORED-CLEAR category which satisfy a cloud test but are restored to clear through additional checks. These two categories of pixel arrays are referred to as "uncertain" pixels in the following discussion.

a) Pixels in the MIXED category:

The first factor that contributes to the uncertain pixels in the MIXED category is the CLAVR-1 condition that if one to three pixels in a 2x2 array satisfy a cloud test, the array is considered MIXED (partly cloudy or mixed overcast). The focus in CLAVR-1 was on the reliability of CLEAR pixels, both over land and over ocean, and this led to a

conservative classification scheme, where all four pixels in the 2x2 array must fail all cloud tests to be classified as CLEAR. These clear conditions are important for retrieval of ocean, land and atmospheric products from AVHRR (McClain et al. 1985, Gutman et al., 1995, Stowe, et al, 1997). To provide these pixel classifications in the real time environment of NOAA/NESDIS, fixed "universal" thresholds are used in a sequence of cloud tests in CLAVR-1 (Stowe et al, 1999). As a consequence, many CLEAR pixels were classified as MIXED because of their proximity to cloud contaminated pixels within the same 2x2 array.

The second factor causing uncertainty in mixed pixels, is the nearest neighbor consistency check in the form of a uniformity test. This test requires that all four pixels in a 2x2 pixel array (adjacent pixels on adjacent scan lines), have radiances which are sufficiently close in reflectance and/or brightness temperature to be classified as CLEAR. This has forced a number of possible clear pixels to be classified as MIXED since only one of the four pixels has to be cloud contaminated to force the array into the MIXED category.

b) Pixels in the RESTORED-CLEAR category:

CLAVR-1 algorithm has a "restoral-to-clear" process whereby a pixel can be moved from MIXED or CLOUDY classification into a RESTORED-CLEAR category. Such restorals occur primarily over daytime oceans and deserts. These restorals have been incorporated into CLAVR-1, based on the realization that for certain combinations of solar and viewing geometries, the CLAVR-1 tests could lead to a MIXED or CLOUD

classification, for a clear scene. For example, in a prescribed angular cone of specular reflection, a pixel might be bright enough, due to the geometry, to be considered cloud, but is restored to clear based on thermal uniformity (Stowe, et al., 1999). However, some clouds are thermally uniform and receive a RESTORED-CLEAR classification by the above process. Thus, RESTORED-CLEAR cannot be assumed to be CLEAR without invoking some additional tests.

Recovering CLEAR pixels from the "uncertain" ones is the objective of the CLAVR-3 algorithm, accomplished by testing these two classes of pixels using dynamic cloud/no-cloud thresholds, which are viewing angle, vegetation type and latitude (illumination angle) dependent.

2.1 CLEAR pixels in CLAVR-1

In this study, spatial average values of the CLEAR albedos and temperatures from CLAVR-1 are computed on regions of approximately 110 km x 110 km (fields). Near the equator, this corresponds to a 1° latitude by 1° longitude region. These approximately 110 km x 110 km equal area regions are called grid cells and they define the spatial extent over which quantities are averaged. At the equator, there are 360 grid cells in each 1° latitude interval, gradually dropping off to 3 grid cells near the poles. There are a total of 41,252 grid cells over the globe and this distribution is referred to as the equal area projection.

a) Nature of CLEAR albedo and temperature fields (Ascending):

Due to the uncertain nature of RESTORED CLEAR samples, only CLEAR pixel arrays in a grid cell are averaged to produce a mean clear albedo and a mean clear

temperature. A clear albedo map for the ascending (mostly daytime) segment of the data for Day 89252 is shown in [Figure 1](#). [NOTE: this is an equal angle (latitude/longitude) representation of the equal area grid]. The *magenta* color, which covers much of the oceans and the poles, indicates that no CLEAR samples are available there. To be consistent with the reflectance thresholds tests used in the CLAVR-1 algorithm, ch. 2 albedo over ocean and ch. 1 albedo over land are used in the figure. Since the purity of CLAVR-1 CLEAR classifications is established (Gutman and Ignatov, 1996), a clear albedo mean is computed even if the sample size is small. Albedo values generally range from 0 to 50% for clear sky cases, with the higher albedos occurring primarily over deserts. Albedos over the oceans are generally in the 5-10% range, highest in the direction of solar specular reflection.

A clear-sky brightness temperature map derived from mean channel 4 radiances for the same day is shown in [Figure 2](#). As expected, regions with no CLEAR samples are identical to those in Figure 1. Mean channel 4 temperatures (T4) over oceans vary between 271°K and about 300°K, while over land, they range between 250°K and 320°K. Global desert areas are clearly discernable from their high temperatures. There is no evidence of cloud contamination (irregular bright or cold patterns) in either figure.

b) Nature of clear temperature distribution (Descending)

During the descending portion of an orbit, only brightness temperatures can be used in CLAVR-3, as most of this portion is in darkness (nighttime). The global distribution of clear T4 from CLAVR-1 during this portion is shown in [Figure 3](#). The temperature scale used is the same as the one used for the ascending part. There is

no noticeable difference from temperatures in [Figure 2](#) over the oceans, but over the land, T4 values are clearly lower at night, as expected due to lower heat capacity of land compared to water. The deserts even appear slightly cooler than the ocean temperatures at night. Temperatures during descending (night) satellite coverage range between 271°K and 300°K over oceans and between 250°K and 300°K over land.

c) CLEAR sample size

Sample sizes of CLEAR, RESTORED-CLEAR, MIXED and CLOUDY categories from CLAVR-1 are shown for day 89252 in [Table 1](#). Data from both ascending and descending satellite passes are shown in the table. Notice that at the pixel level, only 11.6% of the ascending sample and 14.5% of the descending sample are classified as CLEAR. The numbers for ascending are consistent with values obtained by Prince and Goward, 1996 in their analysis using CLAVR flags in Land Pathfinder data. The 'uncertain' group, consisting of MIXED and RESTORED-CLEAR cases, constitutes a major portion of the sample, viz., 49.4% and 40.8% of pixels for ascending and descending portions, respectively.

The distribution of grid cells with CLEAR data (ascending) by water and land area and by grid cell mean albedo (channel 1 for land, 2 for water) is shown in [Table 2](#) for day 89252. The maximum number of clear cells occurs in the albedo range 0-10% over water, while over land, it is in the 10 to 20% range. Also, in contrast to the pixel level case, we note that at the grid cell resolution, 22,464 grid cells (54.5%) contain at least one clear 2x2 pixel array in daytime.

Sample size of clear pixels in grid cells for day 89252 (ascending) is shown in [Figure 4](#). The sample size varies from as low as 4 (one 2x2 array) to as many as 800. The higher numbers generally fall in grid cells that belong to the fair weather regions and in desert areas of the globe, since most samples there are clear. The scarcity of clear samples over the tropical oceans is partly due to cloudiness associated with the Inter-Tropical Convergence Zone (ITCZ) and partly due to the loss of pixels in the region of specular reflection due to the RESTORED-CLEAR classification logic of CLAVR-1. The magenta color indicates no CLEAR observations were present in those grid cells from CLAVR-1 on this day. Note the orbital banding pattern, particularly noticeable over land. This results from pixel area on the Earth increasing as the AVHRR scans away from nadir due to Earth's curvature, so fewer pixels are required to fill equal area grid cells. [Figure 5](#) shows the same information, but for the descending parts of orbits on day 89252. The global distribution appears about the same whether the daytime or nighttime CLAVR-1 algorithm is in use, even though there are almost a million more CLEAR pixels at night (cf. [Table 1](#)).

2.2 Uncertain pixels in CLAVR-1:

Some non-clear grid cells (grid cells with zero clear population) and clear grid cells in [Figure 4](#) contain pixels with uncertain classifications from CLAVR-1. These are either due to the RESTORED-CLEAR or MIXED classifications of pixel arrays.

a) Distribution of RESTORED-CLEAR pixels:

The distribution of mean albedo over the globe from the RESTORED-CLEAR populations is shown in [Figure 6](#). The CLAVR-1 algorithm attempts to recover clear pixel arrays that satisfy cloud tests either in the cone of specular reflection over oceans,

or due to high albedo desert, or snow and ice surfaces. Over the oceans, these RESTORED-CLEAR populations lie along orbital swaths from the western side of each orbit due to the afternoon equator crossing time of the NOAA/11 satellite. However, low lying stratus, which occurs most frequently in regions west of continental masses (Warren et al., 1988), is obviously being classified RESTORED-CLEAR by CLAVR-1, because of the excessively high albedo values there. Stratus clouds in other ocean regions are being similarly classified, as indicated by albedos in excess of 40%. This happens because they are thermally uniform, a condition required of RESTORED-CLEAR pixel arrays. Also, sea ice surfaces poleward of 50° which are bright and cold, may be RESTORED to CLEAR, although on this day from early September. It does not appear to have much of this type of RESTORED-CLEAR. The exceptions are a few grid cells just off the coast of Antarctica and at the very highest latitudes in the Arctic.

Over land, three types of RESTORED-CLEAR arrays are observed: those associated with bright, hot deserts; those associated with hot vegetated land surfaces; and those associated with snow cover. With the exception of snow cover over Antarctica, the locations and magnitudes of the albedos for these RESTORED-CLEAR pixels is consistent with CLEAR classifications in [Figure 1](#). Overall, the RESTORED-CLEAR process in CLAVR-1 is working well for land. [Figure 6](#) shows that these pixel arrays contain additional information about the Earth's surface beyond what is provided in [Figure 1](#), with the exception of those pixel arrays which are contaminated with stratus cloud over oceans.

b) Distribution of MIXED pixels:

A global map of the distribution of MIXED sample average albedo is shown in

Figure 7. In general, albedos of MIXED samples lie between 10 to 25% over the ocean and between 40 and 70% over land areas, which strongly suggests, when compared with the magnitudes and spatial distribution of albedo for CLEAR from Figure 1, that many of these MIXED pixel arrays are cloud contaminated. Unlike Figure 6, a completely random distribution of mixed populations exists over the entire globe.

c) Uncertain Pixel Populations:

The CLAVR-1 algorithm was designed to allow only those pixel arrays that fail all of the cloud tests to be classified CLEAR. The remainder of the pixel arrays were classified either as MIXED, RESTORED-CLEAR (which includes a special subgroup indicating SNOW/ICE), and CLOUDY. The distribution of pixel populations into CLEAR, RESTORED-CLEAR, MIXED and CLOUDY classifications for each 1° latitude zone on day 89252 is shown in Figure 8. This distribution is generally representative of sample size on any given day. CLEAR pixels, shown as diamonds, have a maximum both in the northern and southern hemispheres at latitudes where deserts over land and sub-tropical high-pressure systems over oceans are located. The CLOUDY pixel distribution shows a sharp rise in the number from the equator up to about 70°, and then a decline toward the South Pole. CLOUDY pixels increase in population just north of the equator to about 15° N which corresponds to the ITCZ location in September. It again rises to a peak around 40° N, gradually decreases further northward, until it makes a sharp drop from 80-90° N.

Except near the poles, the largest samples in each latitude zone come from the MIXED pixels. Over most of the globe, the mixed pixels consist of 60 to 70% of the total pixels in a latitude band. The number of RESTORED-CLEAR pixels is generally

small, but reaches a peak between 70° and 90° S, associated with snow over Antarctica (cf. [Figure 6](#)). There are slight increases in RESTORED-CLEAR in the southern and northern sub-tropics probably associated with bright, hot desert locations.

This uncertain category of MIXED and RESTORED-CLEAR cases contains more than 60 to 70% of the total pixels in every 1° latitude zone outside of the polar regions. A reclassification of these pixels is therefore desirable to identify additional clear pixels available for surface and aerosol parameter retrievals, as well as more accurate estimates of cloud cover. The primary objective of this paper is to show how regional, dynamic thresholds, derived from CLEAR observations in CLAVR-1, can be used to select cloud-free (clear) pixels from the uncertain pixel classifications in CLAVR-1.

3.0 DEVELOPING BI-DIRECTIONAL REFLECTANCE AND EMISSION MODELS FOR USE IN RECLASSIFICATION OF UNCERTAIN PIXEL CLASSIFICATIONS

This section discusses the development of clear-sky radiation data sets (CRDS), which are the basic ingredient in the construction of clear-sky radiation thresholds necessary for reclassification. To be effective, these thresholds need to be local, and not global. This is important because albedo and temperature fields are region specific. In particular, clear-sky temperatures can vary significantly from tropics to the polar regions. The thresholds also need to be dynamic because the fields vary with time, particularly temperature, which is highly sensitive to atmospheric dynamics.

In view of this, albedo and temperature statistics for selected AVHRR channel pixels classified as CLEAR are computed for each day in an 8 day period to produce clear-sky radiation data sets (CRDS8). These consist of radiance means and standard deviations along with associated statistics for each equal area (EA) grid cell. During the

8-day interval, means and standard deviations in albedo and temperature vary primarily with changes in satellite zenith angle (SZA), with only minor effects due to solar zenith or azimuth angles, resulting from the sun-synchronous nature of the NOAA polar orbiter. Each day's mean values are used to construct angular dependence models (ADMs) and obtain localized thresholds on albedo and temperature. These thresholds differ substantially from the universal thresholds used in CLAVR-1. Another feature of this approach is that CRDS8 is updated as additional days are processed, and the most recent 8-day statistics are used to construct the ADMs and the associated thresholds. This process makes the ADMs local, dynamic and angle dependent. These dynamic thresholds are used in reclassifying the 'uncertain' pixels described in section 2.

3.1 Rotating 8-day Clear-sky Radiation Data Sets (CRDS8)

The CRDS files are hierarchical in data storage, using samples from CLEAR, RESTORED-CLEAR, MIXED and CLOUDY categories in that order, if samples from a previous category are not available. These files for each day in the satellite repeat cycle (8-days) are gathered in CRDS8. The CRDS8 data set thus contains radiation means, standard deviations, along with maximum and minimum radiation values. It also contains additional parameters like the latitude and longitude of each equal area grid cell, its vegetation type as determined by computing the mean Normalized Difference Vegetation Index (NDVI) [shown to be useful for land cover classification (DeFries and Townshend, 1994)], surface characterization of grid cells as land, ocean, and coastal, and mean satellite zenith (SZA), solar zenith (SZA) and relative azimuth (RAA) angles. Separate CRDS8 files are used for the ascending and descending parts of each orbit. During the ascending part, most of the grid cells have albedo and

temperature statistics from all channels, while during the descending portion, they mostly have temperatures from the infrared channels. Another feature of polar orbiters is the redundant grid cell coverage at higher latitudes. At the equator, each grid cell is viewed by only one orbit. At higher latitudes, some grid cells may be viewed during several consecutive orbits, thus providing several means and standard deviations. In such situations, CRDS chooses statistics from the orbit with the smallest SZA (i.e, most nadir view).

3.2 Building Clear-sky Bidirectional Models

In principle, the CRDS8 file permits development of ADMs (also referred to as bidirectional models) for each grid cell, since data are stored for each grid cell for the past 8-days. But for many cases, particularly those at high latitudes that are frequently cloud covered, clear sky samples may not exist during most or all of the 8 days. Grid cell statistics for the first 8-day period in September 89 indicate that nearly 7,200 of the 42,152 grid cells do not have clear-sky observations for the entire 8 day period. Only 1,500 grid cells have observations for all 8 days. We have therefore clustered the grid cells in a way to obtain sufficient numbers of CLEAR grid cells for different surface type categories.

This is accomplished by choosing a 10° latitude interval as the region for accumulation of grid cell statistics. This interval is large enough to provide enough clear grid cells for creating angle dependent bidirectional models, while small enough to retain characteristic differences due to solar zenith angle and latitude. Further, the grid cells in each 10° latitude interval are broken down into separate vegetation type (VT) categories. All clear grid cells over ocean are put into category 1 (VT=1). Over land,

the bidirectional models are sensitive to surface vegetation which could vary within the 10° latitude interval. This requires a land surface categorization for each grid cell. We have done this with the CLEAR AVHRR radiances by computing a mean NDVI within each grid cell from the channel 1 and 2 clear-sky reflectances.

Vegetation types over land have different reflectances in channel 1 and channel 2 of AVHRR. Using the mean NDVI parameter from the daily CRDS data sets, the monthly mean value for September 1989 is computed. A map of it is shown in [Figure 9](#) (scaled by factor 10). Comparisons with climatological atlases established that the global distribution of vegetation is well represented by this analysis. Generally, as vegetation cover becomes more dense and healthy, the NDVI value for the grid cell becomes more positive. The magenta colored areas represent grid cells where no clear-sky albedos were observed during any day of the month. As an interesting aside, it is also possible to see aerosols over the oceans from the NDVI map. NDVI is negative over oceans because of the spectral redistribution of sun light by molecular scattering, but it is less negative in regions of high aerosol concentrations because of the more spectrally uniform scattering by the larger aerosol particles. These aerosol NDVI patterns are very consistent with other satellite derived distributions of aerosol particles (cf, Husar, et al, 1997).

In order to separate these NDVI values into a few clusters representative of different vegetation types, a frequency distribution of grid cell NDVI monthly mean values over land was constructed from the monthly mean data for September 89, as shown in [Figure 10](#). These values range from -0.50 to +0.55. Six vegetation types (clusters) are identified from modes in the distribution, separated by yellow lines: NDVI

less than 0.0 (VT=2); NDVI between: 0.0 and 0.1 (VT=3); 0.1 and 0.18 (VT=4); 0.18 and 0.25 (VT=5); 0.25 and 0.34 (VT=6); and greater than 0.34 (VT=7). With ocean considered as VT=1, there are a total of seven distinct VT categories.

Thus, each 10° latitude interval consists of grid cells that are classified as belonging to either the water type (VT=1) or one of 6 land types (VT=2 through VT=7). To construct ADMs, daily clear sky albedo and temperature means in each grid cell are sorted by latitude interval, VT value and SZA. They are then combined over an 8 day period in 10° bins of SZA, and albedo and temperature means and standard deviations are computed for each latitude interval and each VT. These means and standard deviations then provide the basis for constructing bidirectional models representing variation in SZA of albedo and temperature for the VT within any latitude interval.

Conceptually, this should result in angular models for 126 combinations of surface type and latitude (18 latitude intervals by 7 vegetation types). However, as results for the ascending portion of day 89252 indicate, clear-sky radiance mean and standard deviation data from slightly more than half the globe (22,464, cf. [Table 2](#)) are available to populate the 126 models. For September, most of these grid cells are located at low and mid latitudes (cf. [Figure 4&6](#)), so CLAVR-3 can only be applied to those regions. Other sources of ADM data (theoretical models, empirical statistics collected over longer time intervals) will have to be used to overcome this deficiency.

During the construction of ADMs for descending portion of orbits, the grid cells maintain their daytime derived VT classifications. It is important to maintain this separation, since different surface types have different emissivities and heat capacities

that affect the angular dependence and magnitudes of the observed brightness temperatures.

3.3 Characteristics of the Clear-sky Models

In the present work, bidirectional models are developed for channel 2 albedo (A_2) and channel 4 brightness temperature (T_4) only. Examples for the first 8-day period, from September 1-September 8, 1989, are shown in Figure 11. [Figure 11\(a\)](#) shows the behavior of the mean (boxes) and standard deviation (asterisk plotted at the mean +1SD for albedo, mean - 1SD for temperature) of A_2 and T_4 for different VT values for latitude interval 8 (10° to 20° South) for ascending data. The three horizontal panels display the SZA dependence of sample size, albedo and temperature, respectively, for each of the VTs. Negative SZA values correspond to viewing the right side of the orbit (away from the sun). Vertical panels present data for VT values 1 through 7, respectively. The ocean (VT=1) has the largest sample size, and is best behaved in its statistical description and angular behavior of the radiative quantities, i.e., smooth angular variations with small standard deviations. Over land in this latitude interval, all VT groups are represented, but the dominant population size comes from VT=4 and 5. The sample size (number of equal area grid cells) generally is smallest near nadir (SZA = 0) due to grid cells having their largest angular size (12° in SZA) there, and smallest angular size at the limb ($\sim 4^\circ$ in SZA). Thus, up to three times as many equal area grid cells may be viewed at the limb than at nadir.

Over ocean, the mean channel 2 albedos are in the range of 2 to 4%, with small standard deviations. A weak specular reflection effect is noticeable at SZA of 25° for

this latitude in September, as is the expected limb brightening due to increased atmospheric scattering along the slant viewing path. The channel 2 albedos are much larger over land. They initially decrease with increasing VT (increasing vegetation cover or greenness), but then tend to increase. Due to the very small sample sizes in VT=2 (NDVI less than 0), variation with SZA is not well behaved. All other land VTs exhibit the expected BRDF pattern with maximum reflectance in the back-scattered direction, further confirming that the CLAVR-1 cloud mask is working well.

Ocean T_4 means are typically lower than land, and all cases except for the poorly sampled VT=2 case, exhibit the expected limb darkening due to water vapor absorption in the 10-12 micron region. Over land, mean temperatures tend to drop with increasing VT, consistent with progressively increasing levels of vegetation that lowers canopy temperatures through evapo-transpiration processes.

For the descending part, the bidirectional models, shown in [Figure 11\(b\)](#), are displayed in the same manner, but the middle panel's albedo values are set to zero because the descending part covers the Earth primarily at night. For every land VT type, the clear-sky temperatures are lower at night than in daytime (Fig. 11(a)), and this diurnal difference is largest for the least vegetated types (lowest VT), consistent with Gutman and Ignatov, 1996. Also limb darkening is suppressed at night for land types due to the radiative effect of lower temperature on the Planck emission function.

4.0 PREDICTION MODELS AND RECLASSIFICATION ALGORITHM

The bidirectional models described in the above section provide a basis for creating the appropriate thresholds for the 9th day following the 8-day period from

which the models were derived. These thresholds represent the most recent clear conditions available and are thus extremely useful for testing whether uncertain pixels from CLAVR-1 are CLEAR. The reclassification algorithm adopted presently is bi-spectral and uses channel 2 albedo, A_2 and channel 4 temperature, T_4 for both water and land.

4.1 Prediction Models

Prediction models developed here provide a statistical description of the behavior of A_2 and T_4 for varying SZA conditions for a given latitude interval and known vegetation type. The albedo prediction model is derived from the bidirectional models by adding one standard deviation to the mean channel 2 albedo ($A_2 \bar{A}_2$) at each mean SZA value $\{(A_p = \bar{A}_2 A_2 + \sigma_A)\}$ (asterisks in Figure 11). The channel 4 standard deviation is subtracted from the mean temperature $\{(T_p = T_4 T_4 - \sigma_T)\}$ to obtain the temperature prediction model. This is done to allow for variation in these two radiative quantities due to the changing conditions over the 8 day period from which they were computed. The sign is chosen to allow that variation to be on the side of cloud contamination, but only by one standard deviation. A multiplier different from unity for the standard deviation may be chosen in future based on more experience or validation against ground-truth field campaigns or other global data sets.

4.2 Reclassification Algorithm

The prediction models provide the most recent, region and vegetation type (VT group) specific thresholds which are also dynamic. In this work, they have only been

used to reclassify pixels with 'uncertain' classifications from CLAVR-1. Thus only RESTORED CLEAR (excluding snow/ice) and MIXED pixels from CLAVR-1 are tested using these dynamic thresholds. Given the SZA value for an "uncertain" pixel from CLAVR-1 located in a grid cell with known VT and latitude interval, the prediction models permit determination of CLEAR/NOT-CLEAR threshold values for channel 2 albedo (A_p) and channel 4 temperature (T_p) during daytime, and for channel 4 temperature (T_p) during nighttime. The observed clear-sky albedo (A_2) and/or temperature (T_4) values for the "uncertain" pixel are compared with these predicted threshold values (A_p and T_p), and a decision is made as to whether the pixel is CLEAR or not. The value of the threshold at the observed SZA is computed by linearly interpolating between two neighboring SZA bins of the corresponding model. Use of polynomial functions to fit the points has been considered and tested, but linear interpolation seems adequate.

CLAVR-1 uses cloud codes in its classification to identify the path followed by the pixel array through the algorithm (Stowe et al., 1999). There are over 40 codes, but they can be grouped into four primary classifications: CLEAR, RESTORED-CLEAR, MIXED and CLOUDY. The distribution of cloud codes among these four classes is shown in [Table 3\(a\)](#). Cloud codes (cc) of 1 through 11 are codes that correspond to CLOUDY conditions, while codes cc = 80-89 are used for cases which are first restored to CLEAR and then back to CLOUDY during the night time. Pixels with cloud code cc = 12 are considered "pure" CLEAR, and form the basis of the ADMs from which the prediction models are computed. RESTORED CLEAR have values of cc = 13-16 over land or water, 30 over deserts and 60-69 during nighttime. The MIXED codes are cc =

17-26 (daytime and nighttime) and 90-99 (nighttime). When CLAVR-1 does not make a decision, cloud code of zero is assigned [note: cc=28,29,31, RESTORED-CLEAR SNOW/ICE are considered missing (as if cc=0) in this application of CLAVR-3 since prediction models for the clear ocean were not reliable at the high latitudes because of excessive cloudiness]. Details on the above CLAVR-1 classifications are described further in Stowe et al., 1999.

The reclassification algorithm is outlined in [Table 3\(b\)](#). If, during daytime, the 'uncertain' pixel albedo, A_2 , is less than the corresponding prediction model's A_p and the pixel temperature, T_4 , is greater than T_p , the pixel is reassigned to CLEAR. If either one of the two tests or both tests are failed, the pixel is either retained as MIXED or reclassified to MIXED. The one exception is the 'RESTORED CLEAR' case with cloud code (cc) of 13. This case usually occurs when viewing spatially uniform marine stratus clouds ($A_2 > 30\%$) in the sun-glint direction. This CLAVR-1 RESTORED CLEAR classification is therefore more correctly classified as CLOUDY in CLAVR-3, rather than as MIXED.

At nighttime, only the temperature threshold test is used. If the temperature test is passed by the pixel, it is considered CLEAR. Otherwise, it is reclassified as MIXED.

If no prediction model is available, RESTORED-CLEAR pixels are assigned to CLEAR; SNOW/ICE and MIXED pixels retain their CLAVR-1 cloud classification.

5. RESULTS OF APPLYING DYNAMIC THRESHOLDS.

Methods described in sections 2 through 4 have been applied to one month of

AVHRR Global Area Coverage (GAC) data for September 1989. The first eight days were processed into the CRDS8 data set to initiate the development of dynamic thresholds for day 9. Subsequently, a new day is processed and the CRDS8 is updated with the previous day, eliminating the oldest day. From the 22-day data set (September 9-September 30, 1989) for which current CLAVR-3 reclassification methodology was applied, results for day 89252 (Sept. 9th) have been selected to illustrate the performance of the CLAVR-3 method. The results are presented in two sub-sections, one for ascending (mostly daytime) and the other for descending (mostly nighttime) satellite overpasses, as the latter only has the benefit of the infrared channels to reclassify uncertain pixels from CLAVR-1. Within each of these subsections, results will be presented to illustrate the impact of CLAVR-3 on the CLEAR pixel and grid cell populations, and on the quality of the CLAVR-3 CLEAR pixel albedos and temperatures through the use of global difference maps (CLAVR-3 - CLAVR-1) and histogram analyses.

5.1 Evaluation of CLAVR-3 performance for Ascending (daytime) data

(a) Quantity of CLEAR Pixels after CLAVR-3 (ascending):

Data from day 89252 were analyzed to determine the increase in clear pixel classifications from CLAVR-3 in relation to CLAVR-1. As shown in [Table 1](#), nearly 50% of the pixels classified from the ascending orbits on this day were in the 'uncertain' (MIXED and RESTORED-CLEAR) category. These are the pixels that were subject to the CLAVR-3 reclassification procedure.

The distribution of pixels after the reclassification is shown in [Table 4](#). Of the 18.2 million samples in the "uncertain" group, albedo and temperature tests were both satisfied for 17.8% of these pixels, and the pixels were reclassified as CLEAR. About 73.7% failed either one or both tests and were not reclassified as CLEAR. There were 8.5% which could not be reclassified because a threshold could not be determined due to lack of a bidirectional model. A total of 3.2 million pixels were added to the CLEAR population after reclassification with CLAVR-3, making the CLEAR population about 20.4% of the total, an increase of 75% over the CLAVR-1 sample.

b) Quantity of CLEAR Grid Cells after CLAVR-3 (ascending):

The change in pixel population due to the addition of CLEAR pixels from CLAVR-3 within grid cells is shown globally in [Figure 12](#). The increase in the number of CLEAR pixels within grid cells can be larger than 600. The increase over oceans is largest along the satellite sub-track, just as the total pixel population is larger there due to pixel area enlargement with increasing viewing angle. This is to be expected, since the uncertain pixels constitute about 50% of the total, and most of these are MIXED. Thus, there is no dependence on position across the orbit, i.e., dependence on solar geometry, as would be the case if RESTORED-CLEAR dominated the uncertain pixels. Thus, the CLEAR pixels from the uncertain population should be expected to have the same sampling pattern as the total population. When compared with [Figure 4](#) (CLAVR-1 grid cell population), one can also see where grid cells with CLEAR pixels have been added by CLAVR-3 (regions colored in [Figure 12](#) that were purple (missing) in [Figure 4](#)).

The number of CLEAR grid cells before and after applying the CLAVR-3 method, sorted by land and ocean, is shown in [Table 5](#). Over oceans, CLEAR grid cells increased by 23.8%, while over land, only by 12.5%. This again is consistent with the fact that a predominant fraction of uncertain classifications are MIXED, and these pixels tend to be more frequently detected over oceans than over land (cf. Stowe, et al, 1999). Globally, CLAVR-3 leads to an increase in CLEAR grid cells by 19.3% (4,340 CLEAR grid cells) over the CLAVR-1 CLEAR grid cell population. As a percent of the total number of grid cells globally (41,252), the number of CLEAR grid cells after CLAVR-3 rose to about 65%, i.e., to nearly two thirds of the globe, compared with about 55% from CLAVR-1. This increased coverage will result in better daily characterization of remotely sensed Earth surface parameters (e.g., SST, Aerosol Optical Thickness [AOT], NDVI) if derived from mean CLEAR grid cell radiances. This approach is used to derive products in the AVHRR Pathfinder Atmosphere project (Stowe and Jacobowitz, 1997).

c) Quality of CLAVR-3 CLEAR Albedos and Temperatures (ascending)

The increased pixel and grid cell populations resulting from CLAVR-3 are only useful if the associated CLEAR radiances (albedos and temperatures) are of comparable quality to those available from CLAVR-1. An albedo difference map (CLAVR-3 - CLAVR-1) is shown in [Figure 13](#). Albedo differences range from -3% to +4%. The coverage in [Figure 13](#) is restricted to those grid cells which were classified CLEAR by CLAVR-1, since the difference is only meaningful if a CLAVR-1 value was observed.

Over oceans, there is no apparent orbital pattern indicating that the CLAVR-3 CLEAR albedos have very similar ranges of magnitude and spatial distribution to the CLAVR-1 albedo map shown in [Figure 1](#). The absence of a specular reflection pattern (orbital banding over ocean) in [Figure 13](#) indicates that CLAVR-3 is reclassifying pixels in this area just as effectively as those outside of it. In the southern hemisphere, the albedo differences are minor and range between -1% and +1%. Over the northern hemisphere oceans, the differences tend to be more positive indicating that CLAVR-3 is allowing pixels with slightly higher albedo into the clear category.

It also appears that CLAVR-3 is correctly interpreting low marine stratus when being viewed in the direction of specular reflection. Otherwise we would see elevated albedos west of continents and at the higher latitudes of the Pacific Ocean, as was observed in the RESTORED-CLEAR map of [Figure 6](#), and increases in grid cell population in these regions in [Figure 12](#). Thus, dynamic thresholds correctly avoid reclassifying these RESTORED-CLEAR pixels from CLAVR-1 as CLEAR.

Over land, the differences tend to be more variable than over ocean, with negative values of at least -2% over the higher albedo surfaces of the Middle East and Southwestern U.S., and positive by as much as +4% over some isolated regions of most continents. Over North and South America, these high positive values tend to cluster around high mountain terrain. This is consistent with these pixels coming from the MIXED classification of CLAVR-1, as evident in [Figure 6](#), caused by large horizontal variability associated with mountainous terrain.

A more quantitative way of visualizing the impact of CLAVR-3 on the quality of

CLEAR albedo (or temperature) is through the use of frequency of occurrence histograms, like the one shown in [Figure 14](#) for albedo over ocean and land, separately. [Figure 14](#) shows the number of grid cells containing CLEAR pixels whose mean albedos range from 0 and 49% in 1% intervals, both before and after the use of dynamic thresholds. CLEAR ocean albedos lie in the range of 1-13%, which is noticeably lower than many of the land values. The number of ocean grid cells that fall in the very low albedo range (1-3%) is very nearly the same in both CLAVR-1 and CLAVR-3. At higher albedos, however, the number of grid cells that contain CLEAR pixels over the ocean at the same albedo value is larger from CLAVR-3. There are no dubiously high values that would invalidate the CLAVR-3 process. The above difference is being caused by the inclusion of more high albedo pixels from the specular reflection regions over ocean by CLAVR-3. The CLAVR-1 pixels constitute a subset of all the CLEAR pixels due to its conservative approach (i.e., minimize chance of cloud contamination) used in developing the algorithm (Stowe, et al., 1999). Thus, addition of other CLEAR pixels that are not part of this subset should be expected to affect grid cell statistics, similar to what is seen in [Figure 14](#).

Additional analyses are required to determine if the CLAVR-1 and CLAVR-3 albedos and temperature grid cell distributions differ significantly. If a statistically significant difference can be established, we might conclude that the CLAVR-3 process is leading to slight cloud contamination in a few cases. If these analyses conclude that there is some cloud contamination, improved methods like choosing other spectral intervals for the threshold tests or other scaling factors for the standard deviation used in computing the thresholds, can be developed.

The redistribution of CLEAR grid cell albedo over land indicates that CLAVR-3 is yielding CLEAR pixel albedos that are unbiased with respect to the CLAVR-1 values, i.e., the distributions look similar. CLAVR-3 generally shows that there are more CLEAR grid cells at each albedo interval. The most frequently occurring albedo value over land is about 12%. The distribution is nearly identical between the two methods above 25% in albedo.

Figure 15 shows the temperature (T4) differences between CLAVR-3 and CLAVR-1. These T4 differences generally range between -3 and +4 °K. Differences tend to be more negative, generally between 0 and -2 °K over the oceans, with values close to -2 appearing more often in the northern hemisphere. The pattern of negative differences in Figure 15 is well correlated with the pattern of positive albedo differences in Figure 13 over oceans, causing concern that some cloud contamination may have been included by the use of CLAVR-3 dynamic thresholds.

Interestingly over land, particularly in mountainous terrain (western U.S. and South America, India, Turkey) CLAVR-3 increases CLEAR temperatures where it increased albedo (cf. Figure 13), which is not symptomatic of cloud contamination. It is consistent with the interpretation that pixels in these grid cells were CLEAR but were classified as MIXED by CLAVR-1, due to horizontal inhomogeneities in albedo and temperature. Other locations over land exhibit small changes in temperature between the two algorithms.

Histograms of grid cell mean T4 (1°K interval) for ascending (daytime) orbital segments from CLAVR-1 and CLAVR-3 are shown separately for land and ocean in

[Figure 16](#). The additional CLEAR grid cells from CLAVR-3 are distributed similar to the albedo distribution shown in [Figure 14](#), with the difference that the redistribution over ocean is skewed towards the cold side, whereas albedo was skewed towards the bright side. This again is consistent with the possibility that CLAVR-3 brings in some cloud contamination over oceans as discussed in connection with albedos. The largest increase in CLEAR grid cells from CLAVR-3 tend to be at temperatures closer to the most frequently occurring values (293°K ocean, 295°K land) from CLAVR-1, which was not the case with albedo.

5.2 Evaluation of CLAVR-3 performance for Descending data

(a) Quantity of CLEAR Pixels after CLAVR-3 (descending):

During the descending portion of orbits, the dynamic thresholds are derived from the temperature ADMs, as only a small fraction of uncertain pixels were observed during daytime conditions, as shown in [Table 6](#). This relaxes the bi-spectral constraint on classification used for ascending data, thus potentially allowing more pixels to be reclassified as CLEAR during the descending segment. Of the 14.5 million uncertain pixels during the descending orbit segments of 89252 (cf. [Table 1](#)), CLAVR-3 method reclassified 4.875 million pixels (33.5%) CLEAR as shown in [Table 6](#). This is almost double the percent reclassified to CLEAR for ascending data (17.8%). The number of descending CLEAR pixels after CLAVR-3 now represents 28.2% of the total pixel population, whereas from CLAVR-1, CLEAR pixels only comprised 14.5% of the total. This corresponds to a 94.9% increase over the CLAVR-1 CLEAR sample size for descending data. About the same number of uncertain pixels as occurred in the ascending case could not be reclassified.

b) Quantity of CLEAR Grid Cells after CLAVR-3 (descending):

Figure 17 shows grid cell pixel population differences during the descending portion of orbits on day 89252. As one would expect, coverage by CLEAR grid cells is more extensive after CLAVR-3. This is due to the addition of grid cells that did not have CLEAR pixel population under CLAVR-1 (cf. Figure 5). The largest increases in grid cells occurs in the southern hemisphere, particularly over oceans, which is opposite the case in the ascending part, where the largest increases occurred in the northern hemisphere. The gains in pixel populations within CLEAR CLAVR-1 grid cells appear to have a similar pattern to the gains in the ascending mode. Maximum increases occur along the sub-satellite track, for the same reason that most uncertain pixels are MIXED and therefore should have distributions peaking where the grid cells are largest relative to the size of the pixels. There are some relatively large increases in the Arctic region for the descending mode which were not present for ascending. This may result from the fact that temperature differences between clouds and clear sky are smaller in this region, making it easier for uncertain pixels to be classified as CLEAR, thus increasing the possibility of some cloud contamination.

c) Quality of CLAVR-3 CLEAR Temperatures (descending):

The differences in mean brightness temperatures between grid cells containing CLEAR pixels from CLAVR-3 and CLAVR-1 are shown in the map of Figure 18. Over land, the differences tend to be near zero with a few isolated instances of positive differences as large as +4°K. These tend to occur where CLAVR-1 CLEAR temperatures were coldest (blue areas in Figure 3), suggesting that CLAVR-3 actually detected some CLEAR pixels missed by CLAVR-1, where the horizontal inhomogeneity

caused these warmer pixels to be classified as MIXED. There are also some isolated instances of negative differences between -1° and -2°K , which tend to surround regions that both algorithms considered CLOUDY (purple areas in the figures). Thus, CLAVR-3 is able to detect clear scenes at the edges of clouds with these negative temperature differences. This indicates that the selection of CLEAR pixels by CLAVR-3 is definitely comparable if not better than CLAVR-1.

Over ocean, more negative differences are evident, particularly in the southern hemisphere. Since clouds tend to be colder than the underlying ocean, this may be indicative of some cloud contamination from CLAVR-3. This was also suspected in the ascending analysis. There are also some isolated instances of positive differences as large as $+4^{\circ}\text{K}$ over oceans. These tend to be in grid cells where CLAVR-1 CLEAR temperatures were lower than surrounding grid cells (dark green areas in [Figure 3](#)). Overall, the quality of the additional CLEAR pixels from CLAVR-3 is in reasonable agreement with those from CLAVR-1, with the exception of a few cases mentioned above.

As further evidence of the quality of CLEAR pixels from CLAVR-3, histograms of the number of CLEAR grid cells from CLAVR-1 and CLAVR-3 in each 1°K temperature interval are shown for ocean and land in [Figure 19](#) for the descending data. As expected, the number of CLEAR grid cells in CLAVR-3 is more at most temperatures. The patterns of the histograms are very similar for ocean and land for descending (nighttime) compared to ascending, where the hot daytime land temperatures were evident. The change in the ocean histogram due to CLAVR-3 is similar to the ascending change, but showing a more pronounced shift to lower temperatures. Again,

the issue of whether this shift to lower temperatures is indicative of possible slight cloud contamination will be the subject of a future investigation.

Over land, contrary to the behavior of histograms for ascending data, CLAVR-3 appears to shift temperatures noticeably to lower values. Further research is required to determine if this is indeed due to cloud contamination, and if so, to implement methods to correct it as discussed before.

The ultimate test of the need to correct for possible cloud contamination will depend upon the use of the CLAVR-3 CLEAR pixels to derive surface and atmospheric parameters, and evaluate if the impact is significant on the derived parameters.

6.0 CONCLUSION AND FUTURE WORK

Bidirectional models for albedo and temperature derived from CLEAR pixel classifications from CLAVR-1 over an 8-day period have been used to search for additional CLEAR pixels from the uncertain (RESTORED CLEAR and MIXED) pixel group in CLAVR-1 for the next day in the sequence. These models provide dynamic, angle dependent albedo and temperature thresholds. This CLAVR-3 method replaces the universal, static thresholds used in CLAVR-1 with dynamic thresholds which represent the most recent (past 8-days) clear-sky albedo and temperature statistics determined from CLAVR-1. This work demonstrates that dynamic thresholds enhance the clear-sky sample sizes both over land and ocean, while essentially maintaining the quality of clear classifications from CLAVR-1. There are indications that the CLAVR-3 reclassifications may be introducing some cloud contamination to the CLEAR albedo

and temperature fields from CLAVR-1. More research is required to understand if contamination exists and if so, to determine the significance of this contamination on derived parameters and to make necessary improvements to the dynamic thresholds used for reclassification.

Stowe et al. (1999) enumerated several problems with the CLAVR-1 scheme and identified regions that are incorrectly classified by the algorithm. Some of these problems are corrected in CLAVR-3. In particular, CLAVR-3 provides increases in CLEAR pixels in the region of ocean specular reflection, where CLAVR-1 assigns a RESTORED-CLEAR (uncertain) classification. Also, pixels over ocean in the regions of low stratus clouds to the west of continents, restored to clear by CLAVR-1, are being correctly left as MIXED or CLOUDY by CLAVR-3. Over land in daytime, mountainous terrain, classified as MIXED by CLAVR-1, are correctly reclassified to CLEAR by CLAVR-3. These added pixels increase both the albedo and temperature in grid cells, a change that is inconsistent with cloud contamination effects.

For the sample day from September, 1989, dynamic thresholds resulted in a 75% increase in CLEAR pixels, from 4.27 million to 7.5 million, during the ascending part and a 95% increase, from 5.14 million to 10.0 million, during the descending part of that day's orbits. This is particularly important for ocean and land surface applications, where reliable identification of clear-sky pixels is necessary for deriving surface parameters like SST, NDVI, AOT, and possibly other surface and atmospheric parameters on a daily basis. As a result of CLAVR-3, 20.4% (ascending) and 28.2% (descending) of the pixels on a given day are being classified as CLEAR compared to 11.6% and 14.5% from CLAVR-1.

Temperature and albedo histograms for land and ocean from CLAVR-1 and CLAVR-3 indicate further that the number of grid cells containing CLEAR radiances is increased, while the mean temperature and albedo distributions remain similar, except that a few of the added pixels may have slight cloud contamination over the oceans.

Future work in this area should emphasize validation of the CLAVR-3 reclassifications with observations from field experiments in regions of sun-glint, low marine clouds and mountainous terrain. Also, as indicated earlier, the current dynamic thresholds have discontinuities at the 10° latitudinal boundaries. Artificial effects caused by these discontinuities can be removed through the use of smoothly changing dynamical thresholds from one latitude interval to the next.

Absence of bidirectional models in some latitude intervals and for some vegetation types is common with an 8-day only clear data set. A process of accumulating data either over longer periods and/or for several repeat cycles, needs to be evaluated to replace the current procedure. Additionally and probably most important, is the use of surface types which are independent of current AVHRR observations and the associated mean NDVI derived from a month of data. Also, snow/ice data sets are required to remove the ambiguity between cloud and CLEAR snow/ice in CLAVR-1, which cannot be addressed by CLAVR-3 because no CLEAR pixels emerge from CLAVR-1 for this condition, and no angular models can be constructed.

ACKNOWLEDGMENTS:

The authors acknowledge the continued help and discussion on the methods and analysis from the members of the CLAVR Science Team. Particular appreciation is due to Gang Luo for graphical support, to Paul Davis and Ken Campana for helpful discussions during the preparation of the manuscript, and to Dan Tarpley and Bill Pichel for a critical review of an earlier version. We also thank Doug Love for coding support during the course of this project and Sreedevi Kumar for her patience in typing multiple revisions of the manuscript. This work was supported with funds from the NOAA Climate and Global Change Program administered by Drs. William Murray and Rex Fleming.

REFERENCES

- Antoine, J.Y., Derrien, M., Harrang, L., Le Borgne, P., Le Gleau, H., and Le Goas, C., 1992: Errors at large satellite zenith angles on AVHRR derived sea surface temperatures, International Journal of Remote Sensing, 13, 1797-1804.
- DeFries, R.S., and Townshend, J.R.G., 1994: NDVI-derived land cover classifications at a global scale, Int. J. Remote Sensing, Vol. 15, 17:3567-3586.
- DeFries, R., Hansen, M., and Townshend, J., 1995: Global discrimination of land cover types from metrics derived from AVHRR Pathfinder data, Remote Sens. Environ., 54, 209-222.
- Davis, P.A., Stowe, L.L., Luo, G., McClain, E.P., Heidinger, A.K., 1999: Automated Generation of global Cloud Datasets from Polar Orbiting Satellites: Part I: CLAVR-2 pixel Scale Multiple Layer Cloud Analyses (MLCA). Jrnl. Atmos. & Ocean. Tech. (In revision)
- Gutman, G. 1989: On the relationship between monthly mean and maximum-value composite normalized vegetation indices. Int. J. Remote Sensing, 10, 8, 1317-1325.
- Gutman, G., Tarpley, D., Ignatov, A., Olson, S., 1995: The Enhanced NOAA Global Land Dataset from the AVHRR. Bull. Amer. Meteor. Soc., 76, 7, 1141-1156.
- Gutman, G., and Ignatov, A., 1996: The relative merit of cloud/clear identifications in the NOAA/NASA Pathfinder AVHRR land 10-day Composites. Int. J. Remote Sensing, 17, 16, 3295-3304.
- Hou, Y.T., Campana, K., Mitchell, K.E., S.K. Yang, and L.L. Stowe, 1993: Comparison of an experimental cloud data set with other observed and forecast cloud data sets, Journal of Atmospheric and Oceanic Technology, 10, 833-849.
- Husar, R.B., Prospero, J.M., and Stowe, L.L., 1997: Characterization of tropospheric aerosols over oceans with the advanced very high resolution radiometer optical thickness operational product, J. Geophys. Res., 102, D14, 16889-16909.

Hutchison, K.D., and Hardy, K.R., 1995: Threshold functions for automated cloud analyses of global meteorological satellite imagery, 1995, Int. J. Remote Sensing, Vol. 16, 18:3665-3680.

Luo, G., Stowe, L.L., and Davis, P.A., 1999: An inter-comparison of total and layered cloud amount between CLAVR, ISCCP, and MSMR for November 28, 1991 FIRE-II region, J. Atmos. & Oceanic Tech., (in revision).

McClain, E.P., Pichel, W.G., and Walton, C.C., 1985: Comparative performance of AVHRR-based multichannel sea surface temperatures, Journal of Geophysical Research, 6, 11587-11601.

McMillin, L.M., and Crosby, D.S., 1984: Theory and validation of multiple window sea surface temperature technique, J. Geophys. Res., 89, 3655-3661.

Prince, S.D., and S.N.Goward, 1996: Evaluation of the NOAA/NASA Pathfinder AVHRR Land Data Set for global primary production modeling, Int. J. Remote Sensing, 17, 1, 217-221.

Stowe, L.L., McClain, E.P., Carey, R., et al. 1991: Global distribution of cloud cover derived from NOAA/AVHRR operational satellite data, Adv. Space Res., 11,51-54.

Stowe, L.L., Vemury, S., and Anne, V.R., 1993: AVHRR Clear sky Radiation Data Sets at NOAA/NESDIS. Adv. Space Res., 14, 1, 113-116.

Stowe, L.L., P.Davis, and E.P.McClain, 1995:Evaluating the CLAVR (Clouds from AVHRR) Phase I cloud cover experimental product, Adv. Space Res., 16, 10, 21-24.

Stowe, L.L., A.M. Ignatov, R.R. Singh, 1997: Development, validation and potential enhancements to the second generation operational aerosol product at NOAA/NESDIS. J. Geophys. Res., 102. D14, 16,923 -16,934

Stowe, L, and H. Jacobowitz, 1997: The AVHRR Pathfinder Atmosphere Project. Proceedings 9th Atmospheric Radiation Symposium, AMS, Boston, MA. pp. 196-197.

Stowe, L.L., Davis, P.A., and McClain, E.P., 1999: Global cloud cover from AVHRR data, Part I - Development and case study evaluation of the CLAVR-1

algorithm, Jrnl. Atmos. & Oceanic Tech. (Accepted)

Suttles, J.T., R.N.Green, P.Minnis, G.L.Smith, W.F.Staylor, B.A.Wielicki, I.J.Walker, D.F.Young, V.R.Taylor and L.L.Stowe, 1988: Angular Radiation Models for Earth-Atmosphere System, Vol. I - Short wave radiation. NASA Ref. Pub. 1184, Washington, DC. 147 pp.

Taylor, V.R., and Stowe, L.L., 1984: Reflectance characteristics of uniform earth and cloud surfaces derived from Nimbus-7 ERB, J. Geophys. Res., 89, 4981-4996.

Vemury, S., L. Stowe P. Davis and V. Anne, 1997: Classification Improvement using dynamical cloud/no-cloud thresholds from clear-sky radiation data. Proceedings 9th Atmospheric Radiation Symposium, AMS, Boston, MA., 355-357.

Warren, S.G., C.J.Hahn, J.London, R.M.Chervin and R.L.Jenne, 1988: Global distribution of total cloud cover and cloud type amounts over the ocean, NCAR Technical Notes. NCAR/TN-317+STR/DOE, Tech. Rep. ER-0406. 42 pp. + 170 maps. [NTIS number DE90-00-3187].

Wu, A., Li, Z., and Cihlar, J., 1995: Effects of landcover type and greenness on advanced very high resolution radiometer bidirectional reflectance: Analysis and removal, J. Geophys. Res., 100, D5: 9179-9192.

FIGURE CAPTIONS

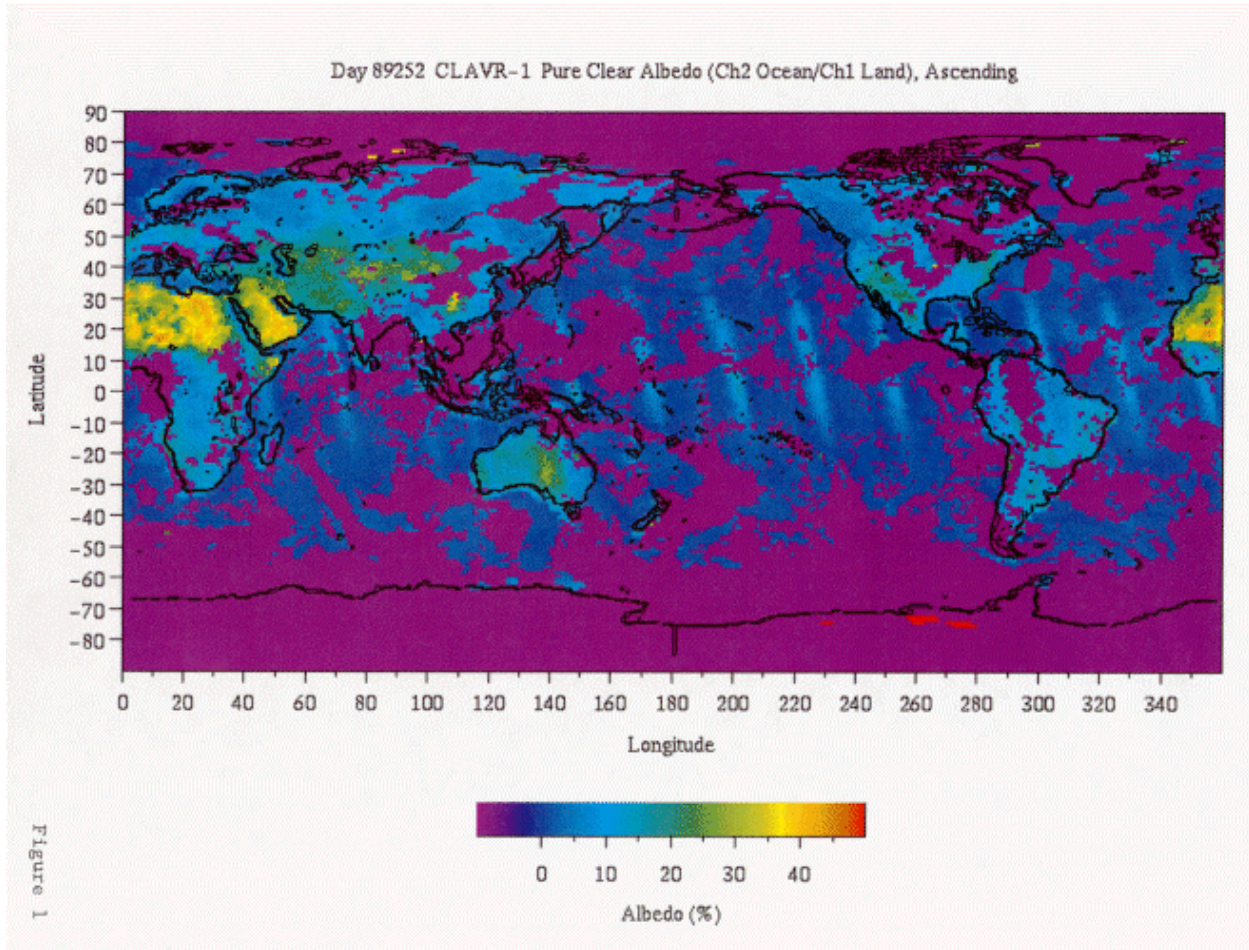


Figure 1: Global distribution of channel 1 of channel 2 albedo means for clear sky conditions as determined by CLAVR-1. Albedo averages are created at 110km x 110km equal area resolution and converted to an equal angle lat/lon projection. Over land, channel 1 albedos are used and over ocean, channel 2 albedos are used. Data for day (89252; September 9, 1989). Ascending parts of orbits.

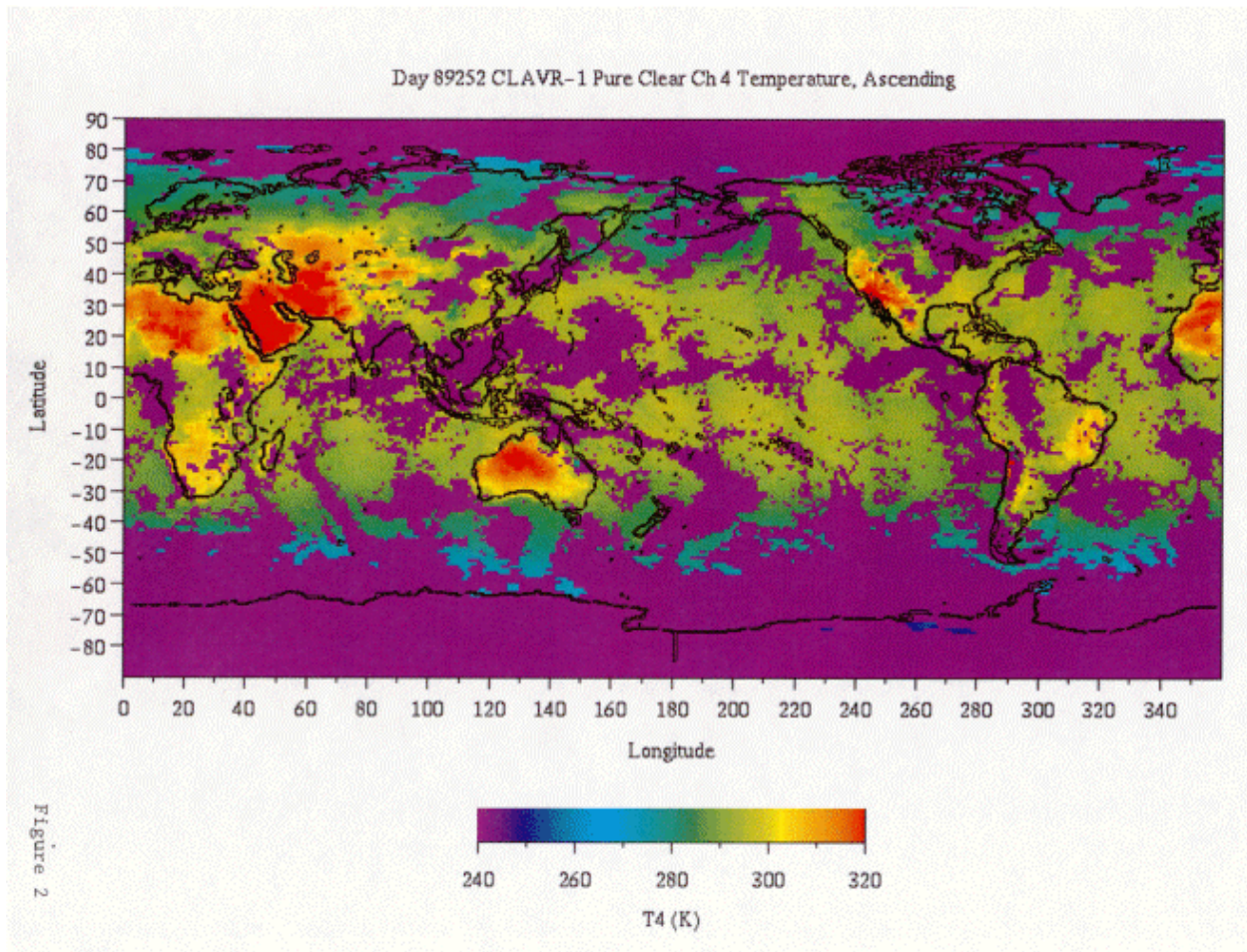


Figure 2: Same as Figure 1 for channel 4 temperature means for clear sky conditions. Ascending parts of orbits.

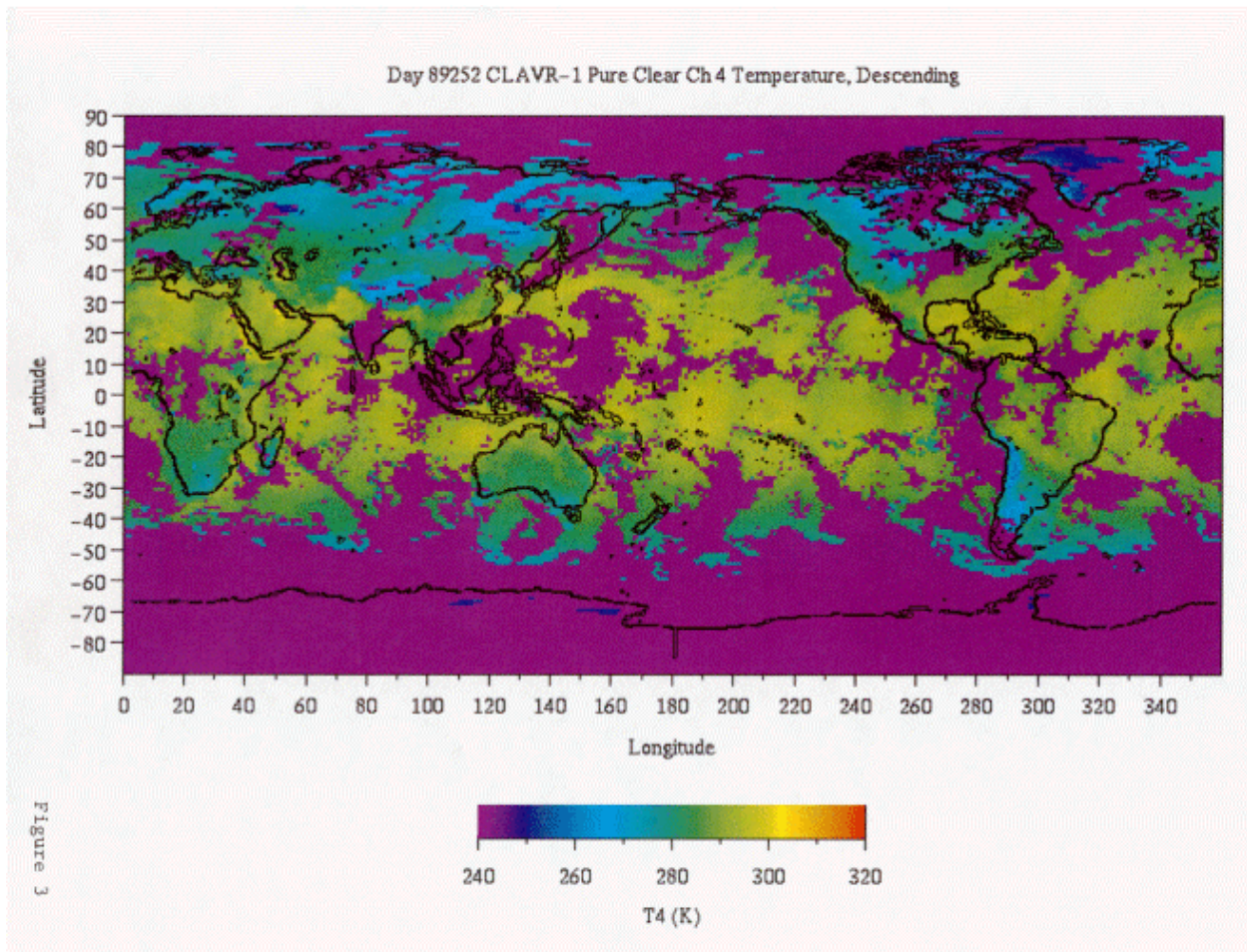


Figure 3: Same as Figure 2 for clear sky conditions. Descending parts of orbits.

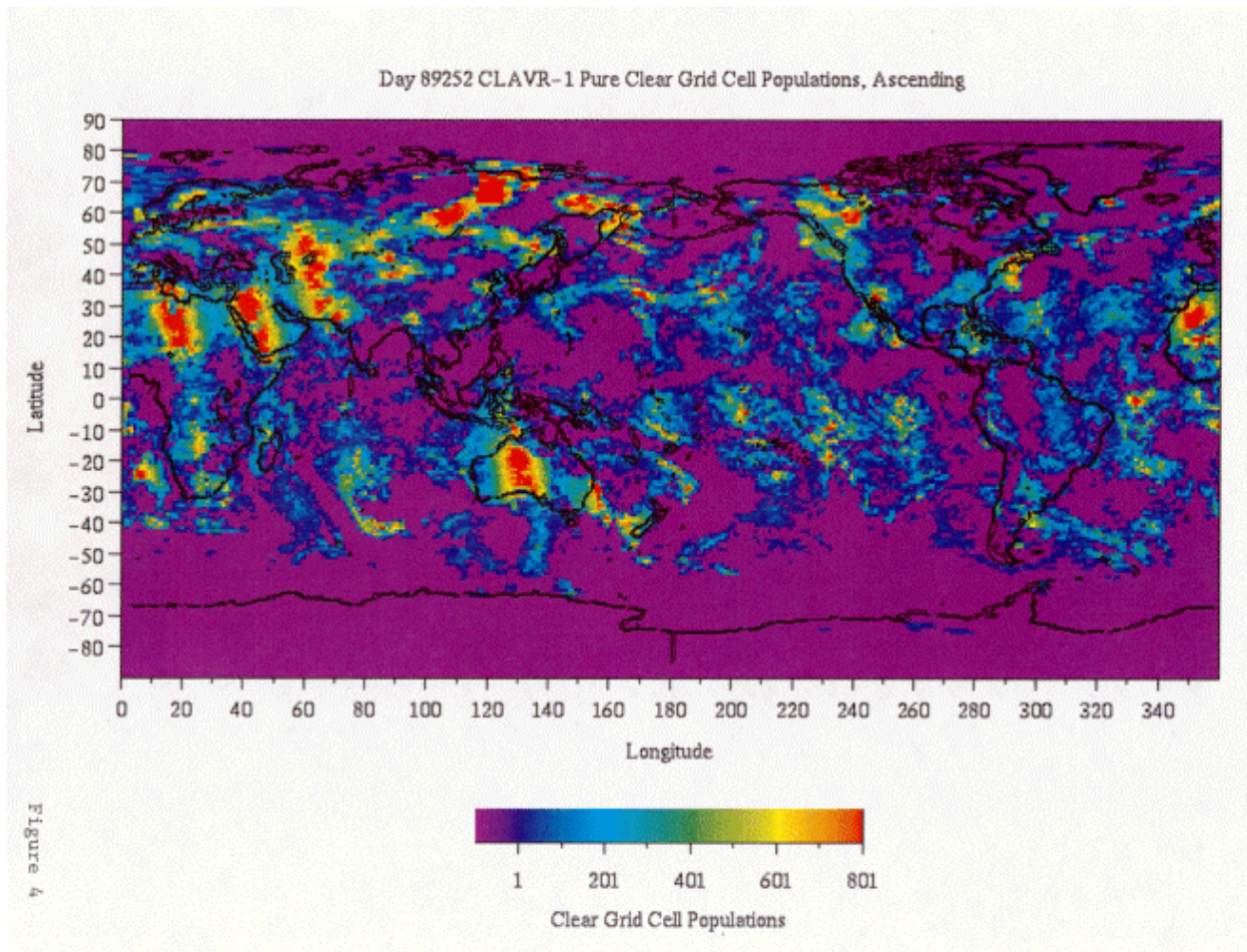


Figure 4: Global distribution of grid cell pixel populations for CLAVR-1 clear cases. Data for day 89252. Ascending parts of orbits.

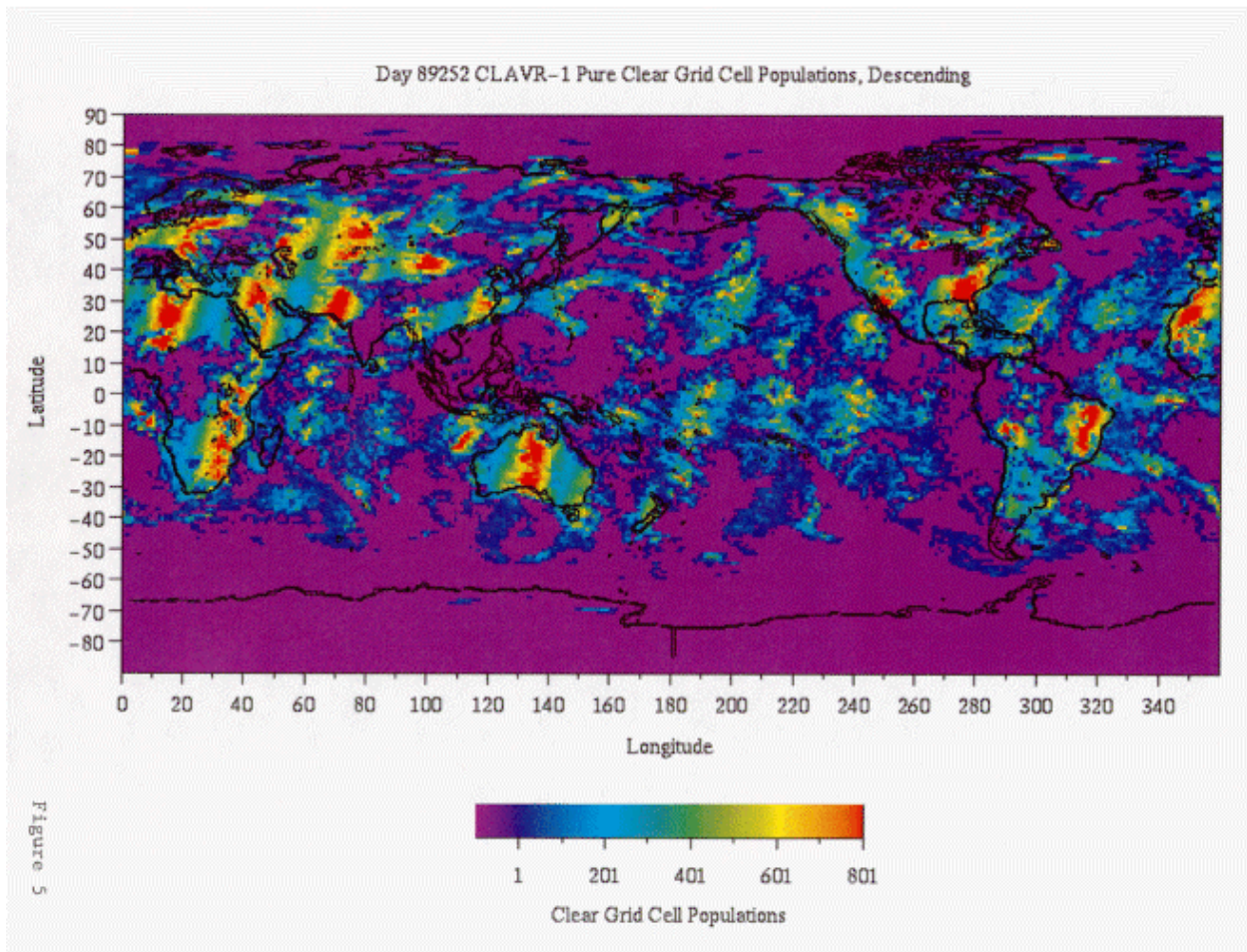


Figure 5: Same as Figure 4 but for descending data for 89252.

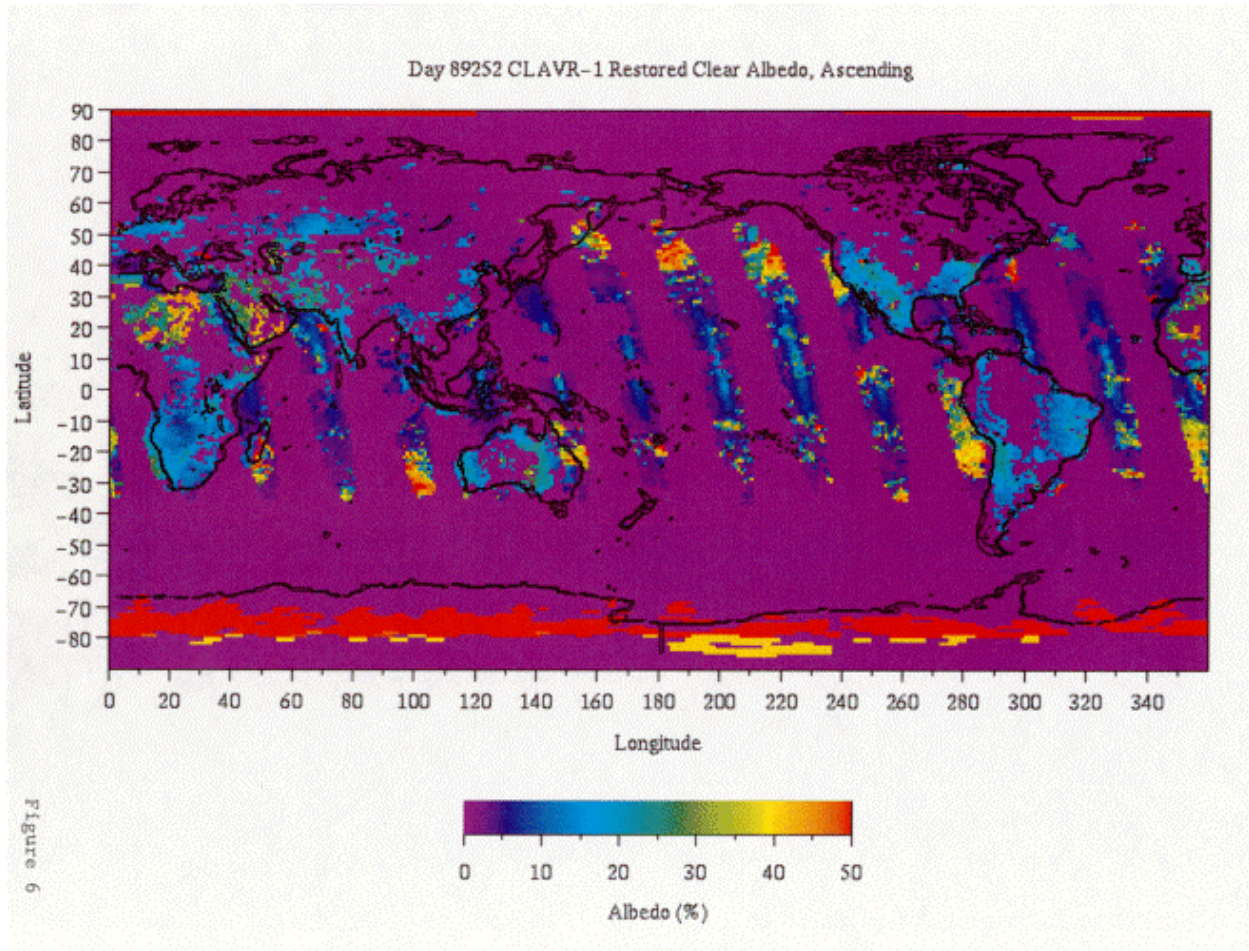


Figure 6: Same as Figure 1 for grid cells with RESTORED CLEAR samples.

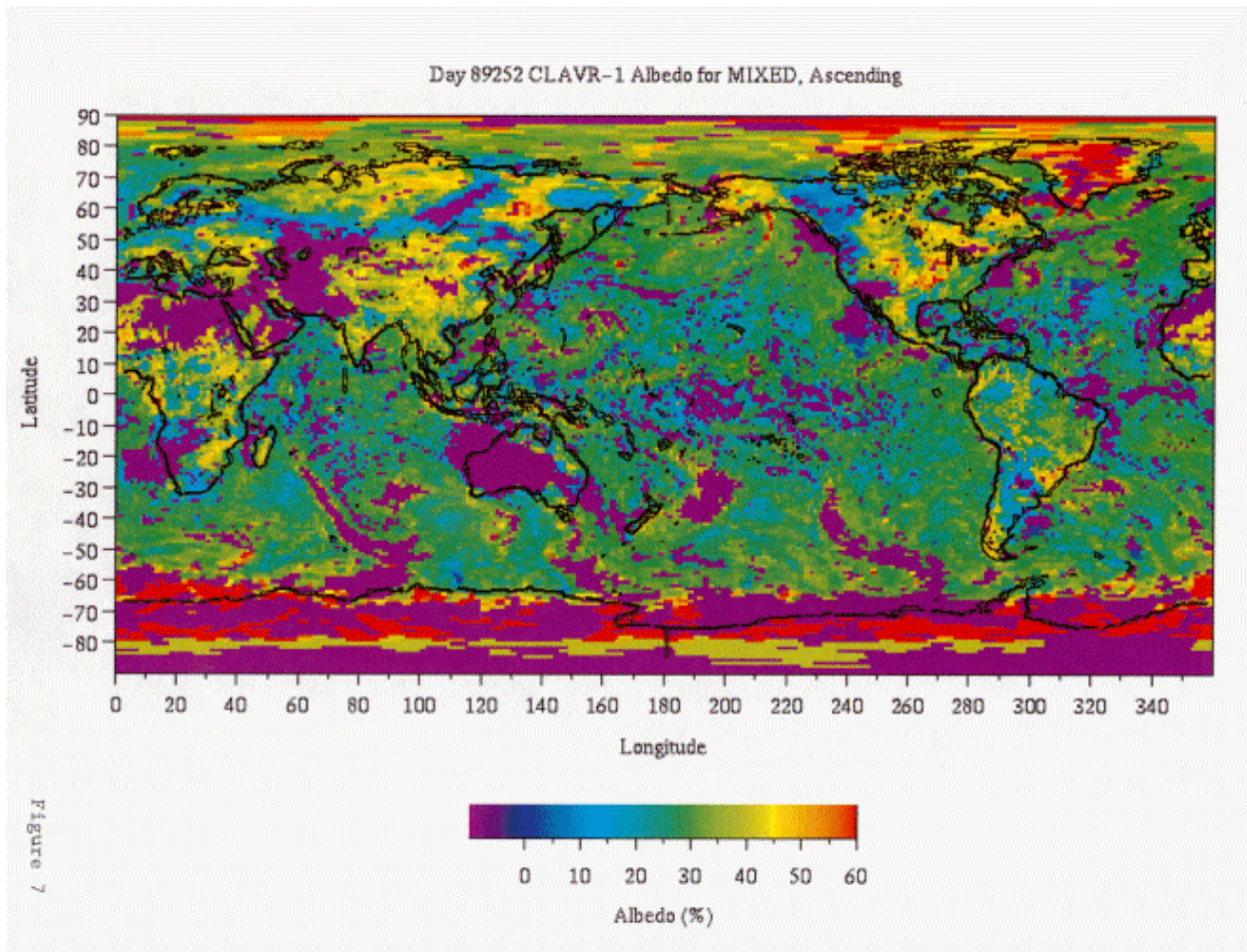


Figure 7: Same as Figure 1 for grid cells with MIXED samples.

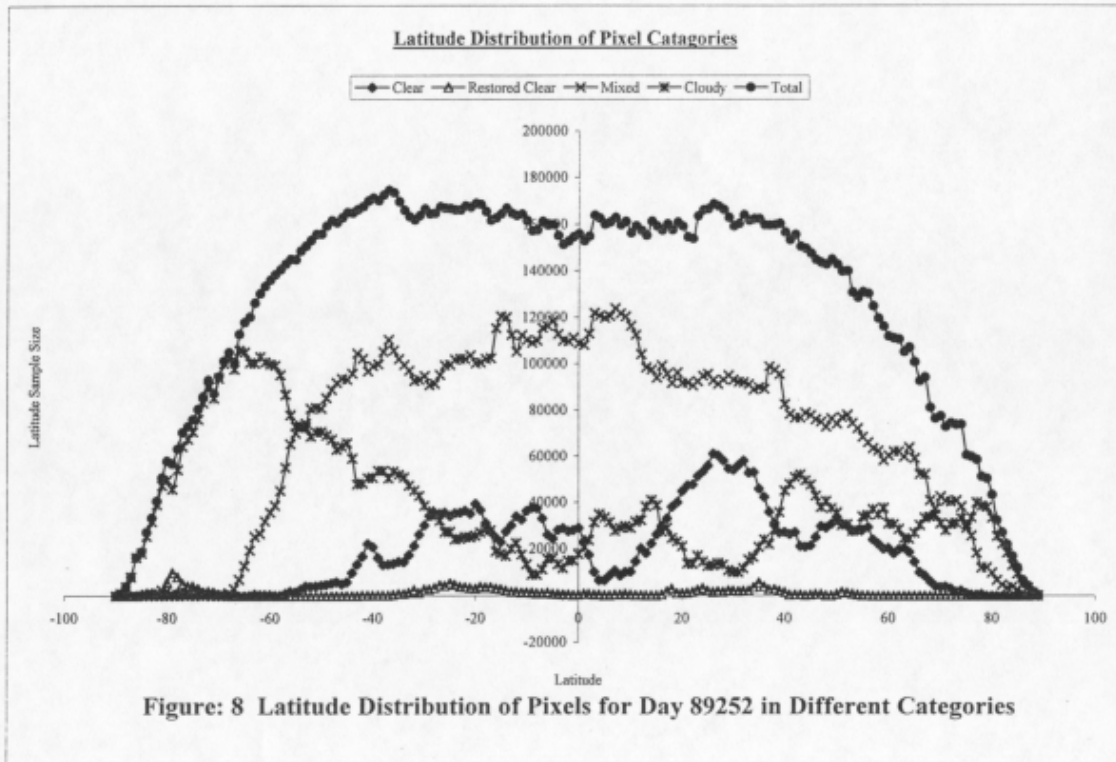


Figure: 8 Latitude Distribution of Pixels for Day 89252 in Different Categories

Figure 8: Zonal distribution of total pixel population counts for day 89252, ascending parts of orbits from CLAVR-1. Distribution of the total sample into each 1° latitude band into CLEAR, RESTORED-CLEAR, MIXED and CLOUDY categories is shown. Population count is shown as ordinate and latitude intervals from -90° (south) to +90° (north) on the abscissa.

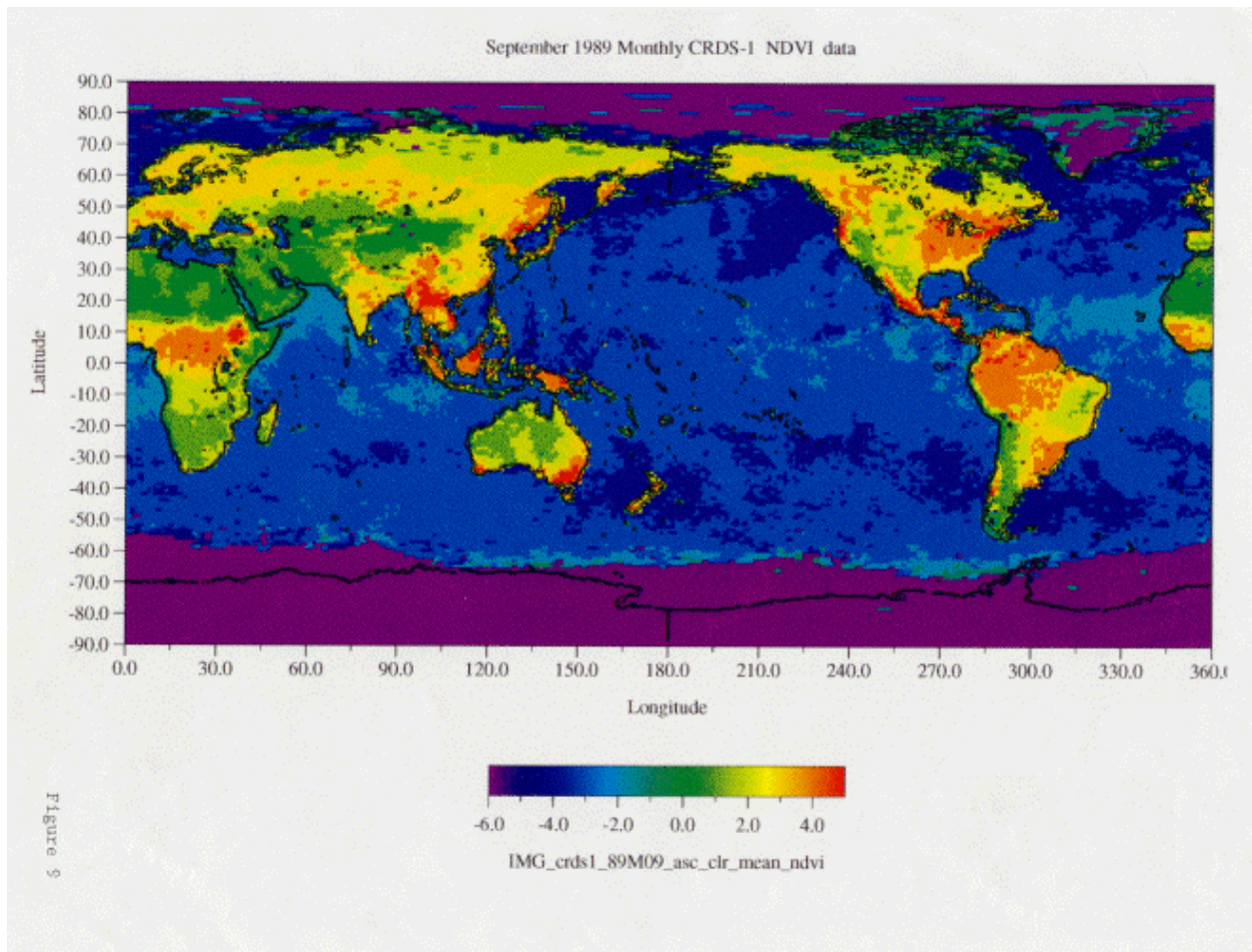


Figure 9: Global distribution of grid cell monthly mean NDVI derived from CLEAR data for September 1989 from CLAVR-1. The data shown correspond to $\text{NDVI} \times 10$.

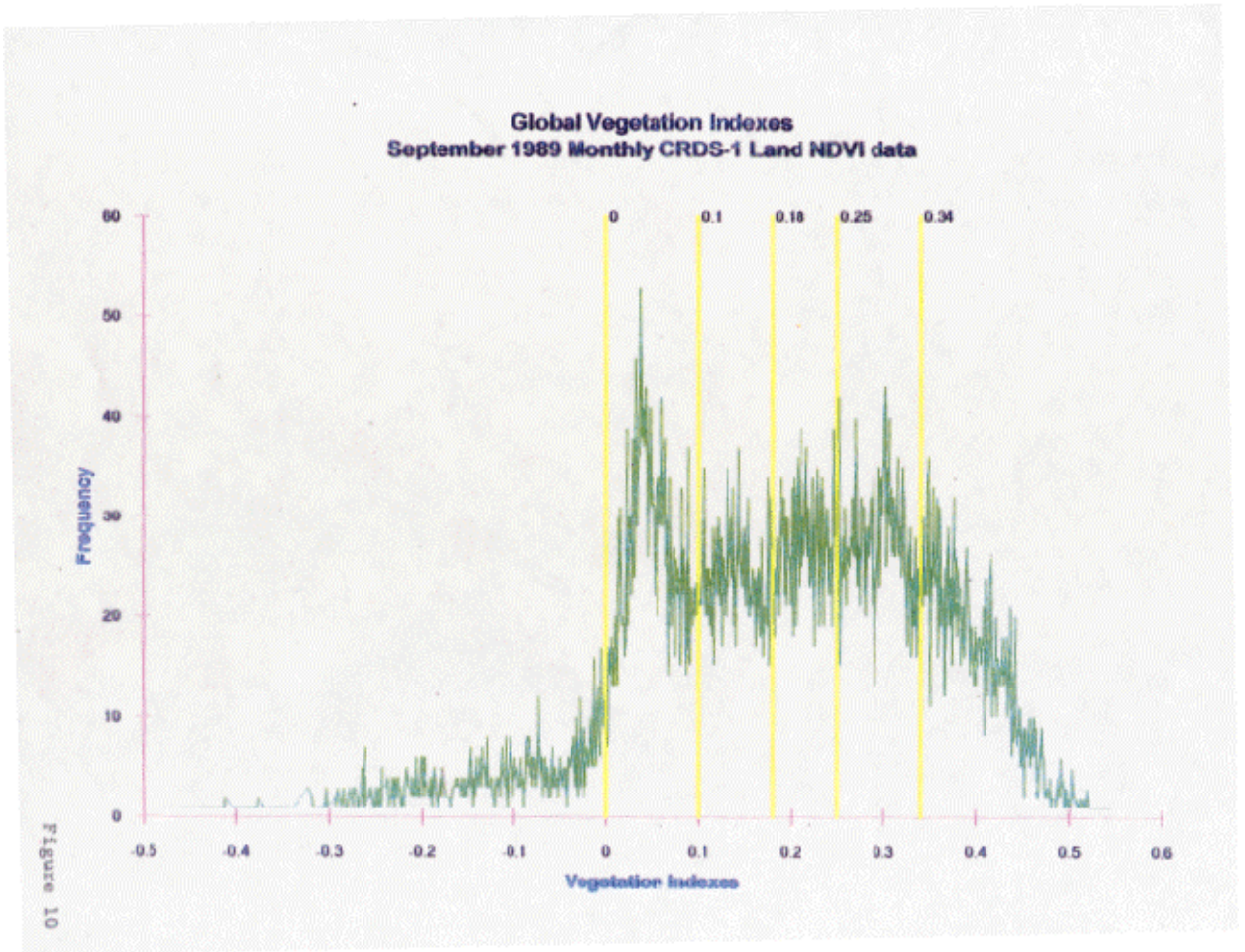


Figure 10: Frequency of occurrence of grid cell monthly mean NDVI for September, 1989.

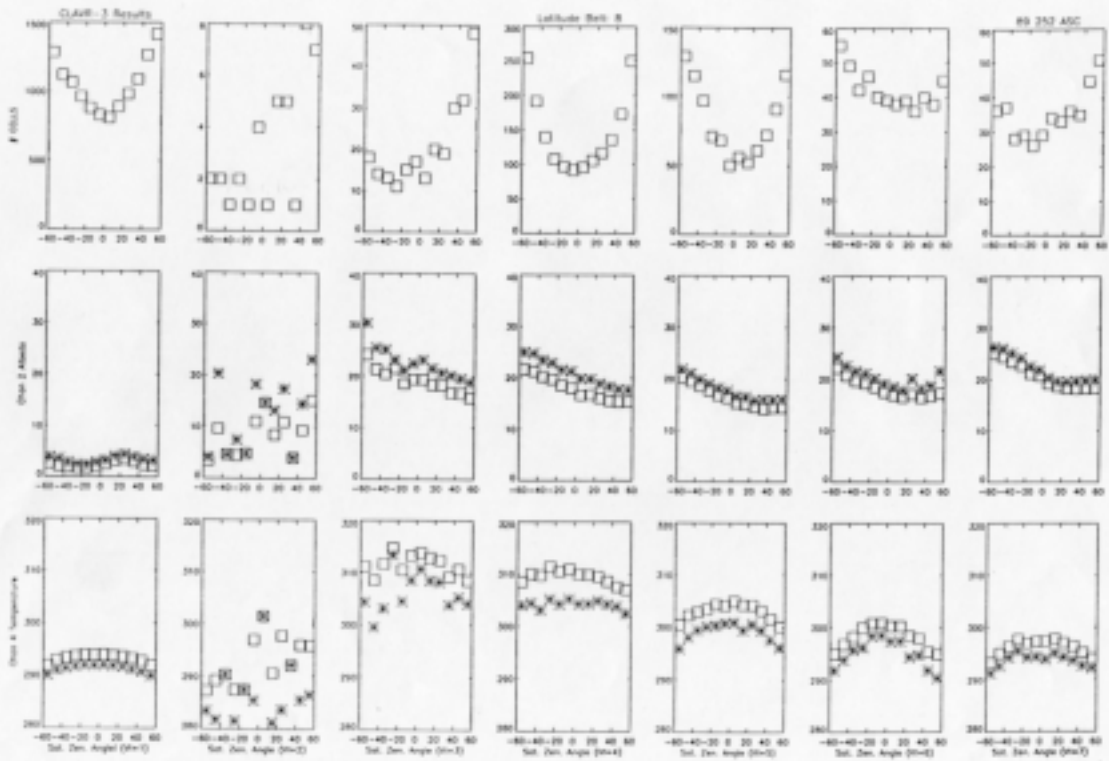


Figure 11(a): Albedo (A_2) and Temperature (T_4) Bidirectional Models for Latitude Interval 8 (10°S-20°S) - Ascending

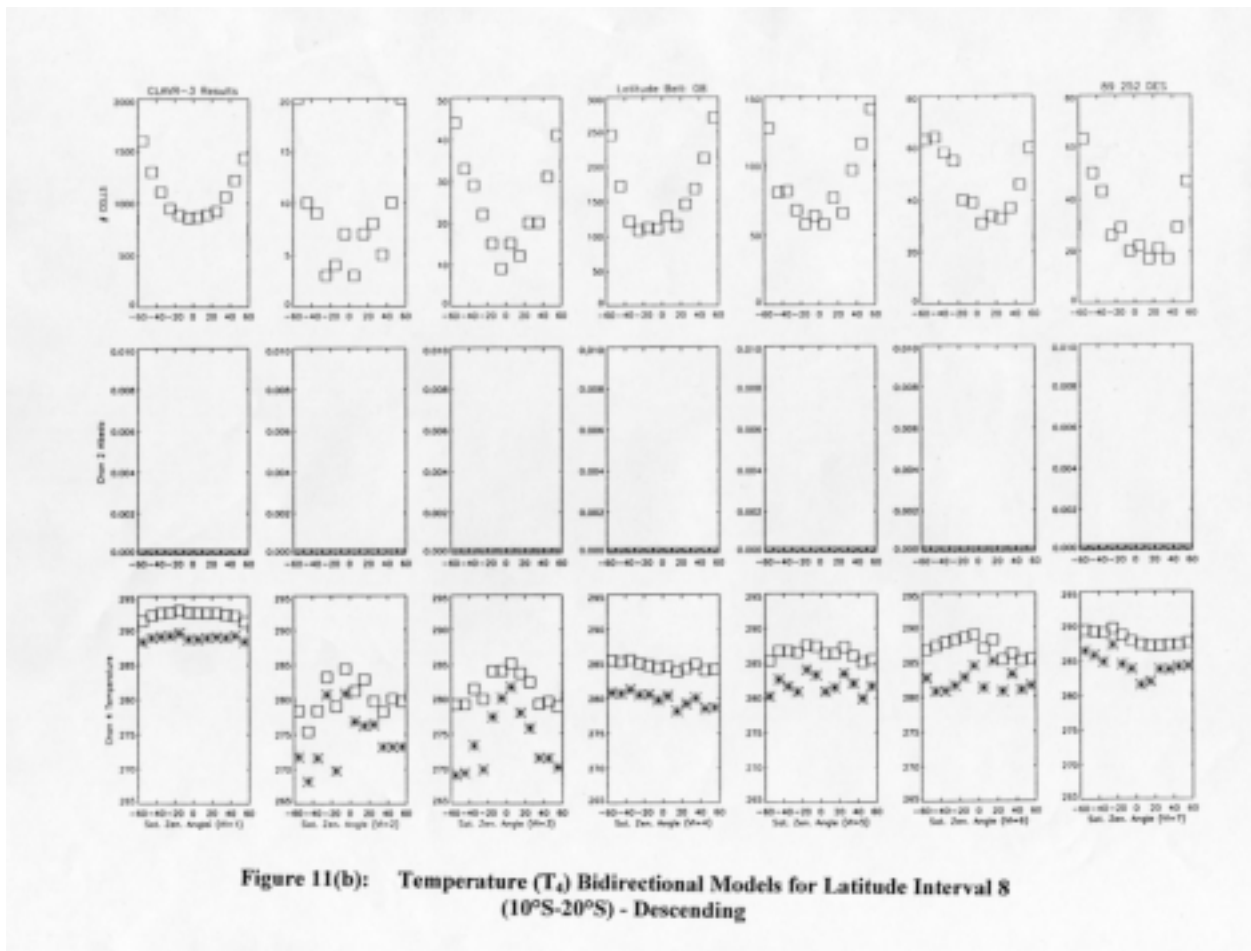


Figure 11(b): Temperature (T_d) Bidirectional Models for Latitude Interval 8 (10°S-20°S) - Descending

Figure 11: Reflection and emission patterns (ADMs) from CLEAR albedo and temperature means in grid cell as a function of satellite zenith angle. Panel 1 has number of grid cells, panel 2 has albedos and panel 3 has temperatures.

- (a) for latitude interval 8 (10°S to 20°S), Ascending;
- (b) for latitude interval 8, Descending.

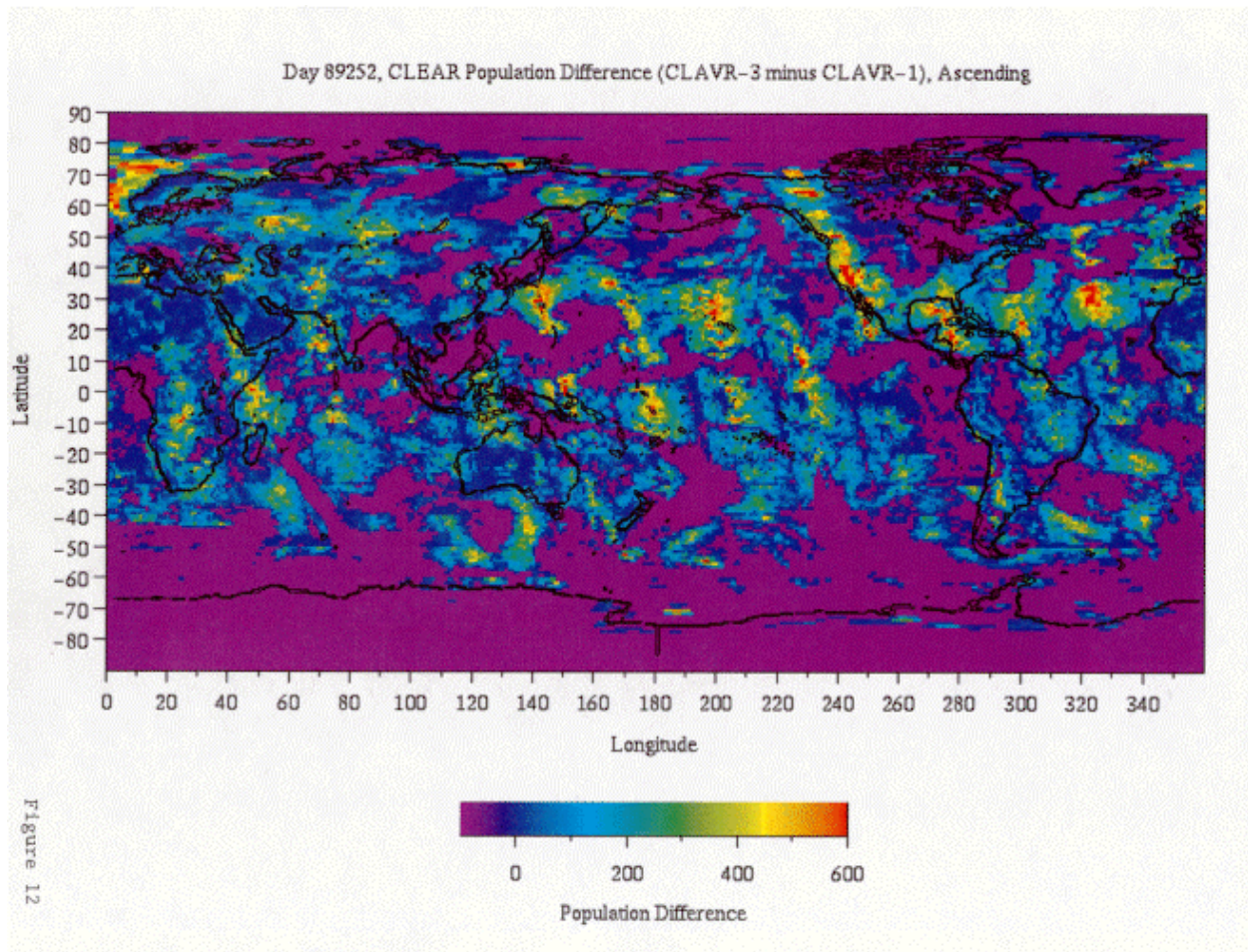


Figure 12: Difference in CLEAR pixel population in grid cells between CLAVR-3 and CLAVR-1, shown in lat-lon projection for ascending data, 89252.

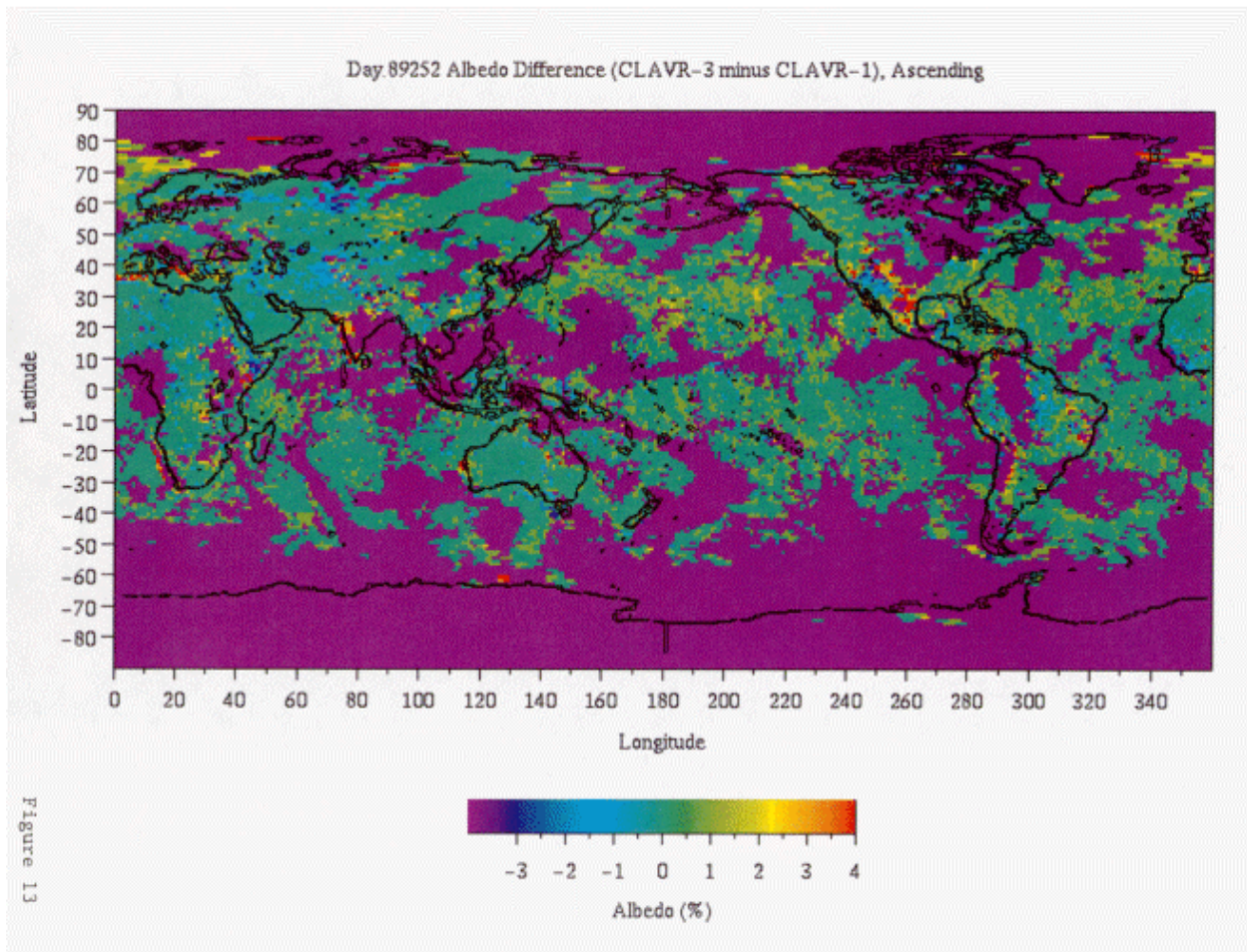


Figure 13: Same as Figure 12 but differences are grid cell mean albedos between CLAVR-3 and CLAVR-1.

HISTOGRAM OF NUMBER OF GRIDCELLS (ASCENDING)
ALBEDO

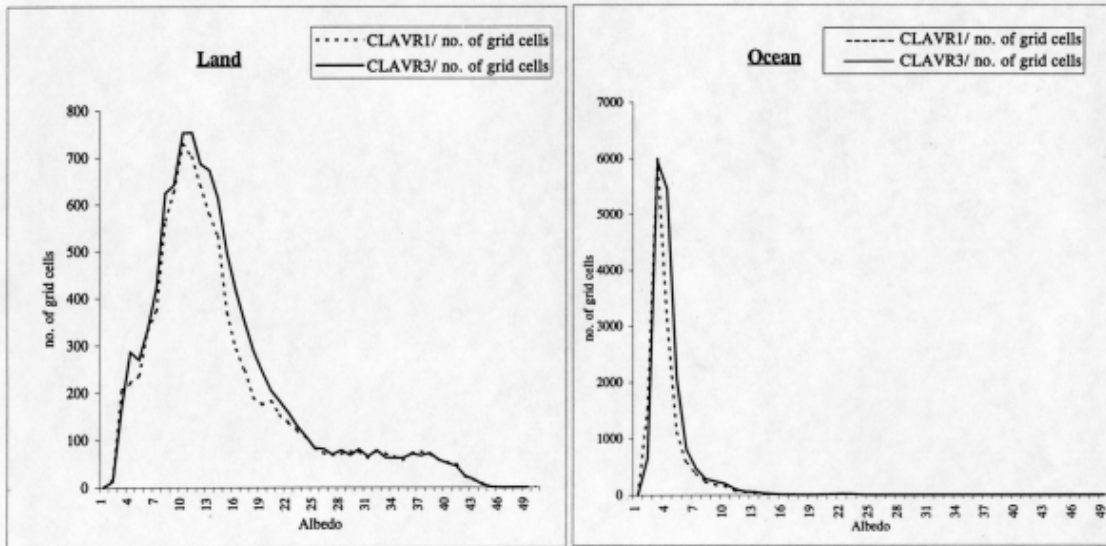


Figure: 14

clavr1&3 albedo Ocean vs land(Asc.)Dec98

Figure 14: Histograms of number of clear grid cells in 1% albedo intervals over ocean and land for ascending case. CLAVR-1 results are shown as dashed and CLAVR-3 as solid line.

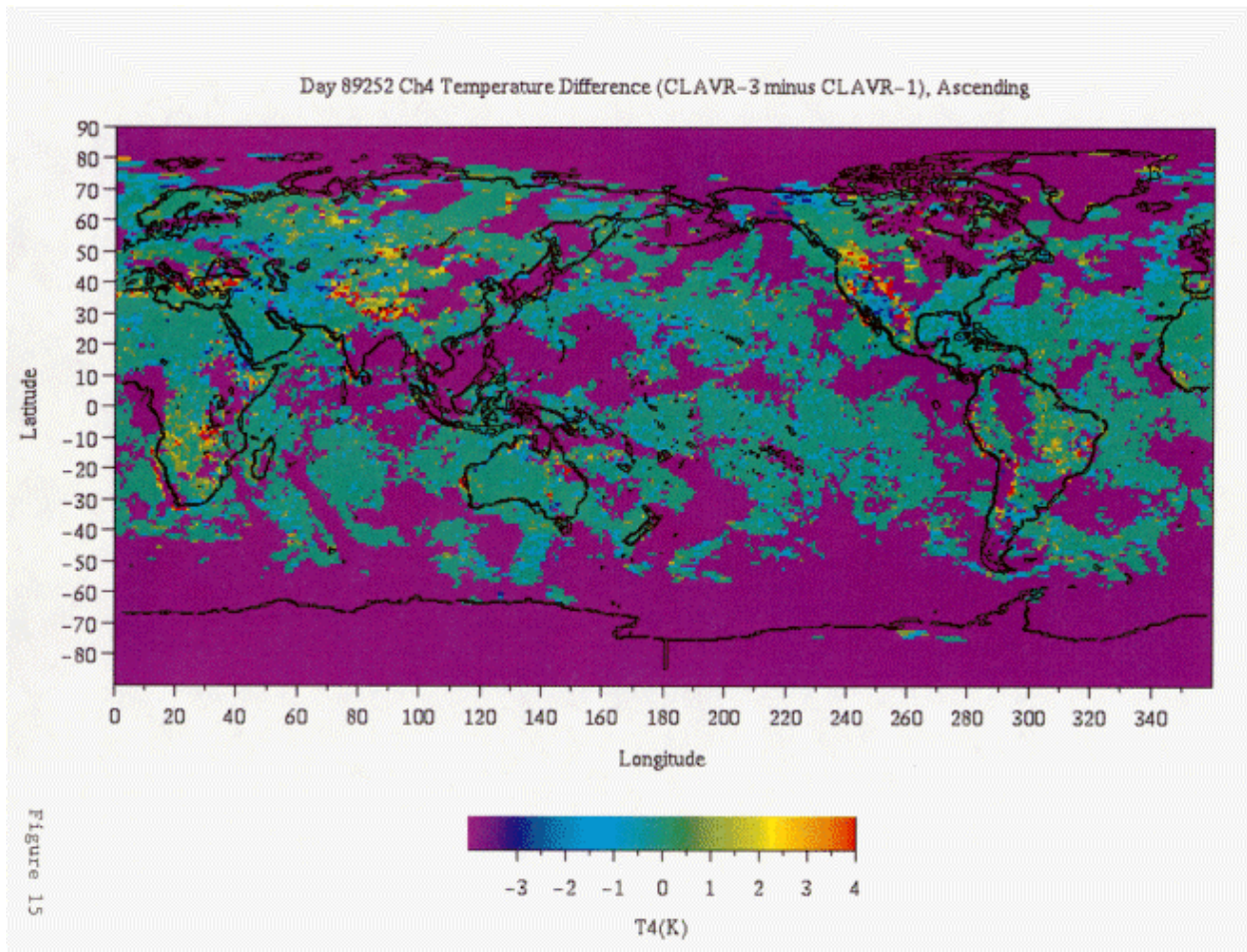
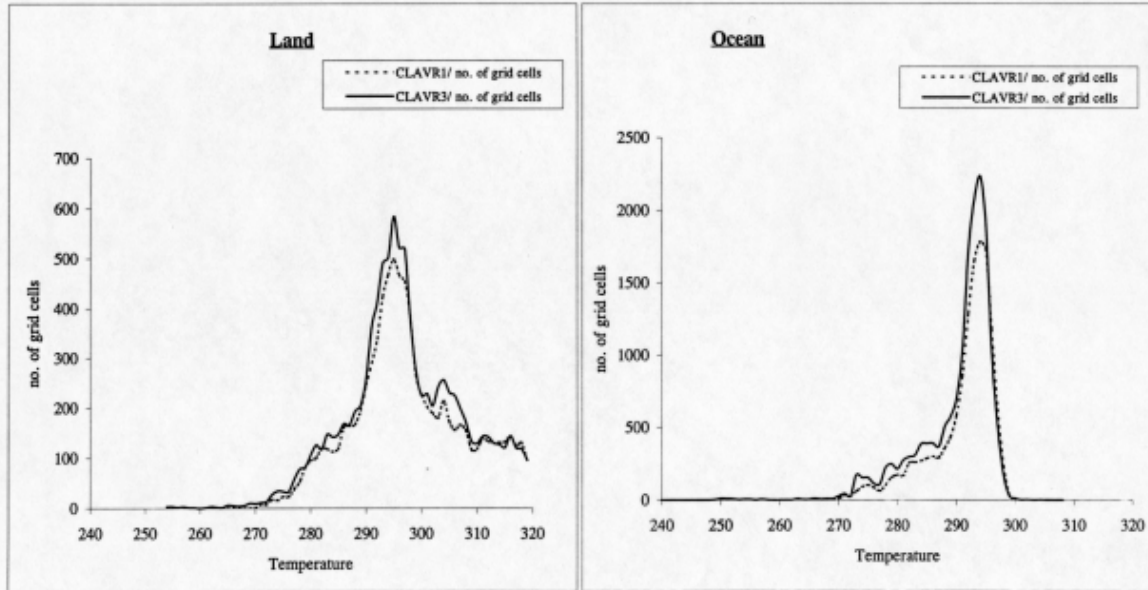


Figure 15: Same as Figure 12 but for grid cell mean temperature differences.

HISTOGRAM OF NUMBER OF GRIDCELLS (ASCENDING)
TEMPERATURE



Jan.99

Figure: 16

clavr1&3 temp Ocean vs land/Asc. jan99

Figure 16: Histograms of number of clear grid cells in 1°K temperature intervals over ocean and land for ascending case. CLAVR-1 results are shown as dashed and CLAVR-3 as solid line.

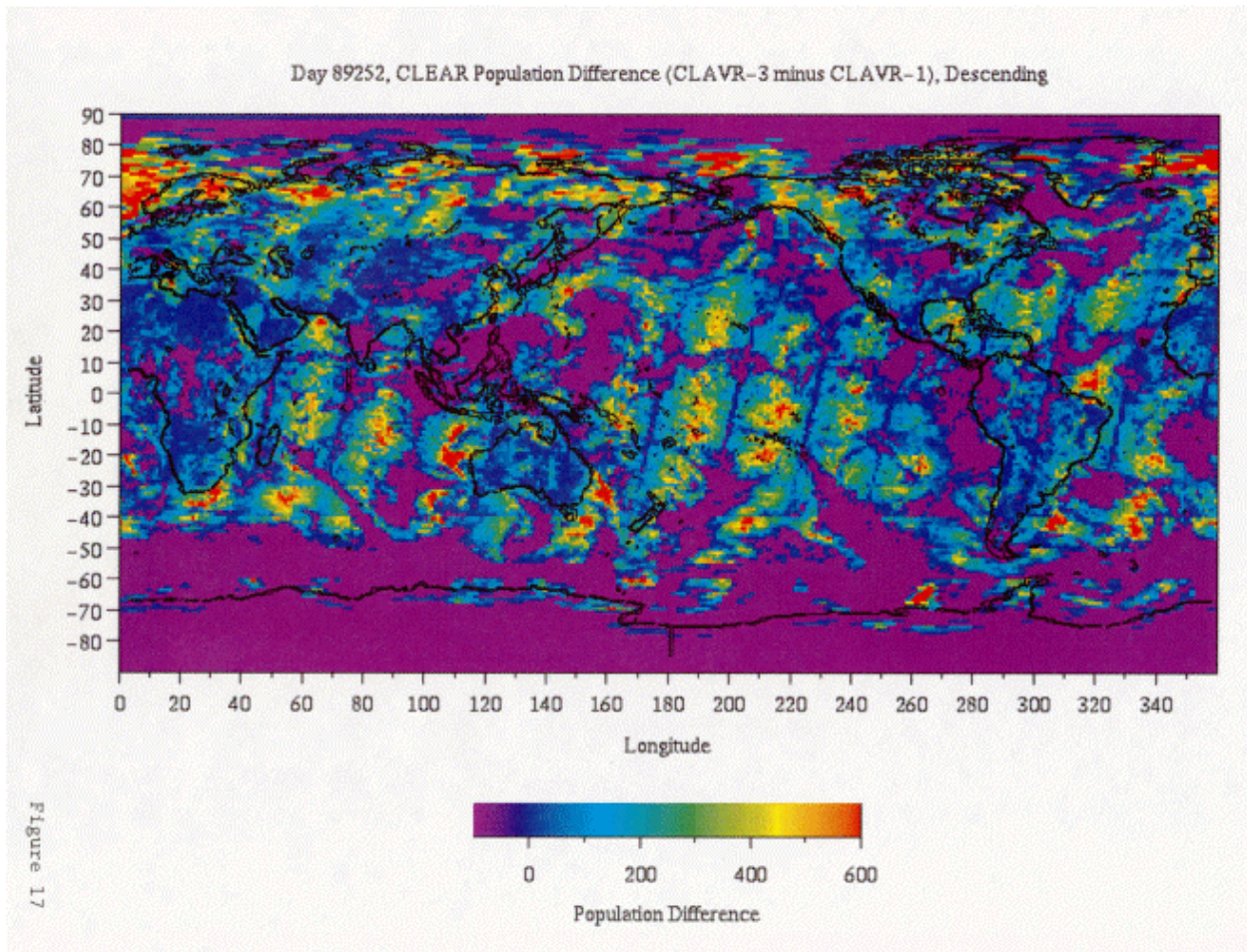


Figure 17: Same as Figure 12 but for descending data on 89252.

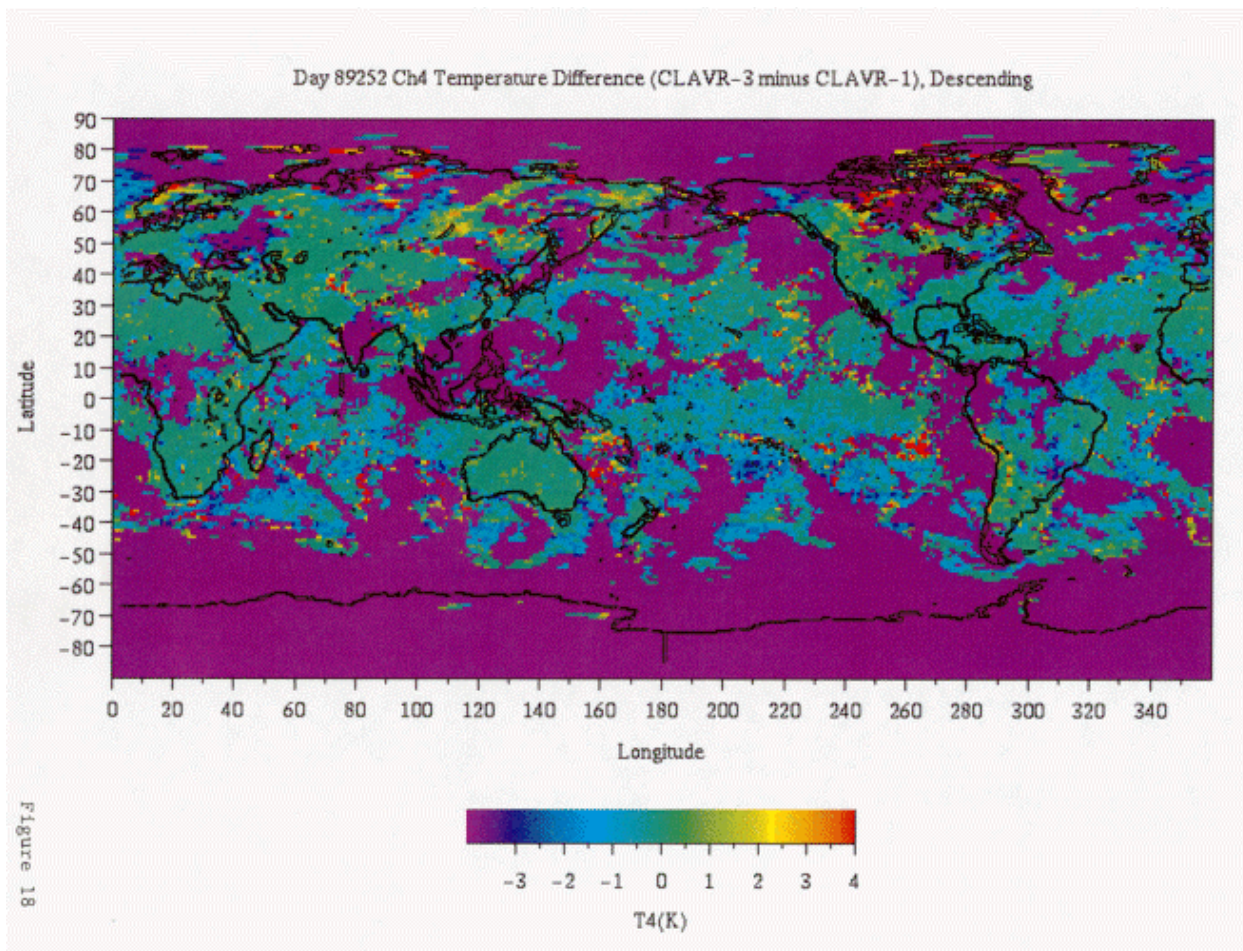


Figure 18: Same as Figure 15 but for descending data.

HISTOGRAM OF NUMBER OF GRIDCELLS (DESCENDING)
TEMPERATURE

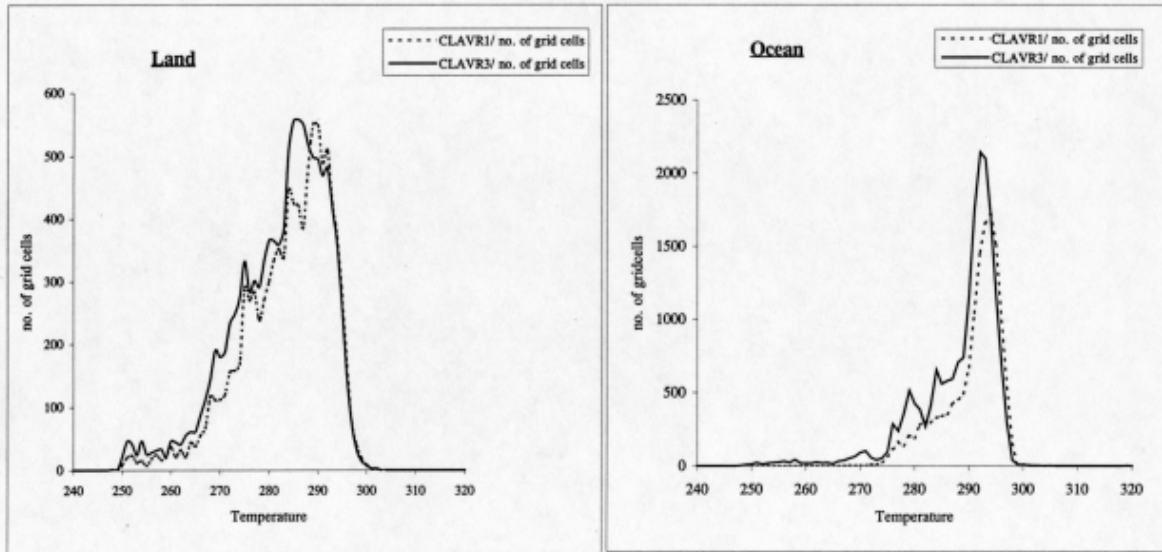


Figure: 19

clavr1&3 temp land vs ocean/Temp: 1998

Figure 19: Same as Figure 16 but for descending data.

LIST OF TABLES

Table 1

CLAVR-1 CLASSIFICATIONS

Day 252, 1989

CATEGORY	ASCENDING		DESCENDING	
	No. of pixels	Percent	No. of pixels	Percent
Clear	4,269,242	11.6%	5,139,734	14.5%
Restored Clear	1,111,764	3.0%	120,284	0.3%
Mixed	17,100,152	46.4%	14,416,189	40.5%
Cloudy	14,404,698	39.0%	15,892,690	44.7%
Total	36,885,856	100%	35,568,897	100%

Table 1: Global sample size of pixels in CLEAR, RESTORED-CLEAR, MIXED, and CLOUDY categories for the ascending and descending portions of orbits from CLAVR-1 output for September 9, 1989 (Day 89252).

Table 2
Pure Clear Grid Cell Counts (CLAVR-1)

Pure Clear Albedo (%)	No. of Water Grid Cells Ch 2	No. of Land Grid Cells Ch 1	Total
0-10	13,289	3,311	16,600
10-20	220	3,909	4,129
20-30	2	962	964
30-40	0	662	662
40-50	1	96	97
50-60		0	0
>60		12	12
TOTAL	13,512	8,952	22,464
% of Global grid cells	32.8%	21.7%	54.5%

Table 2: Population of equal area grid cells containing CLEAR pixels from CLAVR-1 in 10% albedo intervals. Water and land grid cells are shown separately for ascending data.

Table 3

Mixed and Restored Pixel Re-Processing Approach

(a) CLAVR-1 Color Code Decisions	
No Decision	cc = 0
Overcast	cc = 1,11; 80-89 (night)
Pure Clear	cc = 12
Clear over Snow	cc = 28, 29, 31
Restored Clear	cc = 13 - 16; 30; 60 - 69 (night)
Mixed	cc = 17 - 27; 90-99 (night)

(b) CLAVR - 3 REPROCESSING ALGORITHM	
LA = latitude index	
VT = vegetation type	
$A_p(LA, VT) = \bar{A}_2 + \sigma A_2$	
$T_p(LA, VT) = \bar{T}_4 - \sigma T_4$	

RESTORED CLEAR (cc = 13-16; 30)	
If ($A_2 < A_p$) and ($T_4 > T_p$), Then CLEAR, Else	$\left\{ \begin{array}{l} \text{MIXED (cc = 14,16)} \\ \text{CLOUDY (cc = 13)} \end{array} \right.$
RESTORED CLEAR (cc = 60 - 69) - Night time	
If ($T_4 > T_p$), Then CLEAR, Else MIXED	

MIXED (cc = 17 - 27)	
If ($A_2 < A_p$) and ($T_4 > T_p$), Then CLEAR, Else MIXED	
MIXED (cc = 90-99) - Night time	
If ($T_4 > T_p$), Then CLEAR, Else MIXED	

NO ADM: RESTORED → CLEAR	MIXED → MIXED

Table 3: CLAVR-3 MIXED and RESTORED-CLEAR pixel reprocessing approach:

- (a) Original CLAVR-1 cloud codes and classifications.
- (b) CLAVR-3 reprocessing algorithm.

Table 4

**CLAVR-3 Reclassification Statistics
1989, Day 252, Ascending
Total Uncertain Pixels Reclassified
(Mixed and Restored Clear: 18,211,916)**

CLAVR-3 Reclassifi- cation	DAYTIME PIXELS		Night Time Pixels	Total	Percentage Uncertain Pixels
	Both Channels	Either Channel			
No. of Pixels (Clear)	3,232,229		5,211	3,237,440	17.8%
No. of Pixels (Mixed or Cloudy)	9,658,555	3,678,384	87,293	13,424,237	73.7%
No. not Reclassified				1,550,239	8.5%

Table 4: Pixel statistics for MIXED and RESTORED-CLEAR cases after reclassification with CLAVR-3 for ascending data. Percent of 'uncertain' pixels reclassified into categories: "CLEAR", "MIXED or CLOUDY", and "NOT RECLASSIFIED" (due to lack of models) is shown for ascending data from 89252.

Table 5

**Change in Number of Clear Grid Cells
after Dynamic Thresholds (Ascending)**

Surface Type	Before CLAVR3	After CLAVR3	% Increase
Ocean	13,512	16,730	23.8%
Land	8,952	10,074	12.5%
Total	22,464	26,804	19.3%
% of Global Grid Cells	54.55%	64.98%	

Table 5: Number of clear grid cells over land and ocean before and after use of dynamic thresholds for ascending data from day 89252. The percent increase as a result of CLAVR-3 is also shown.

Table 6

**CLAVR-3 Reclassification Statistics
1989, Day 252, Descending**

**Total Uncertain Pixels Reclassified
(Mixed and Restored Clear: 14,536,473)**

CLAVR-3 Reclassifi- cation	DAYTIME PIXELS		Night Time Pixels	Total	Percentage Uncertain Pixels
	Both Channels	Either Channel			
No. of Pixels (Clear)	848		4,874,712	4,875,560	33.5%
No. of Pixels (Mixed or Cloudy)	70,052	43,410	8,312,159	8,425,621	58.0%
No. not Reclassified				1,235,292	8.5%

Table 6: Same as Table 4 but for descending data. Note that just as ascending data has some nighttime pixels, descending data has some daytime pixels.